Image Cover Sheet

CLASSIFICATION	SYSTEM NUMBER
UNCLASSIFIED	508057

TITLE

ENHANCEMENTS TO AVAST

System Number:

Patron Number:

Requester:

Notes:

DSIS Use only:

Deliver to:

National Defence
Research and Development Branch

Défense nationale
Bureau de recherche et développement

DREA CR/96/421

ENHANCEMENTS
to
AVAST

D.P. Brennan — M.W. Chernuka

MARTEC Limited
1888 Brunswick Street, Suite 400
Halifax, Nova Scotia, Canada
B3J 3J8

CONTRACTOR REPORT

Prepared for

Defence Research Establishment Atlantic

Centre de Recherches pour la Défense Atlantique

Canada

National Defence
Research and Development Branch

Défense nationale
Bureau de recherche et développement

DREA CR/96/421

ENHANCEMENTS to AVAST

D.P. Brennan — M.W. Chernuka

MARTEC Limited
1888 Brunswick Street, Suite 400
Halifax, Nova Scotia, Canada
B3J 3J8

Accepted by :
Layton Gilroy - Contract Scientific Authority

March 1996

W7707-5-3369/01-HAL
Contract Number

CONTRACTOR REPORT

Defence Research Establishment Atlantic

Centre de Recherches pour la Défense Atlantique

Canada

ABSTRACT

The development and incorporation of the latest enhancements to the AVAST code are described. The purpose of this work was to make the modelling of the physical environment more realistic, while ensuring that the code runs as efficiently as possible. To this end, several new features have been added. These include the implementation of a four-noded acoustic panel element and the development of an eigenvalue extraction technique suitable for equations generated by the boundary integral equation method. In addition, the option to use structural response data generated by the COUPLE program has also been incorporated.

TABLE OF CONTENTS

LIST OF TABLES

LIST OF FIGURES

LIST OF FIGURES - Continued

1. INTRODUCTION

Phases I through IV of the DREA/Martec collaborative investigation in underwater acoustics has resulted in the development of a series of computer programs, collectively named AVAST, for the numerical prediction of the acoustic radiation from submerged elastic structures immersed in either infinite, half-space or finite depth fluid domains. AVAST combines both the finite element method for the structure and the boundary integral equation technique for the fluid. The finite element method (FEM) is used to define the mechanical mobility matrix relationship between excitation forces (in a particular direction and at a particular frequency) and structural velocities at fluid/structure interface nodes. The boundary integral equation method (BIEM) is used to generate a system of equations relating surface velocities to fluid acoustic pressures.

In an attempt to make the modelling of sound radiated from submerged structures more realistic, several enhancements have recently been incorporated into the previously existing AVAST suite. These include the development and implementation of a four-noded fluid panel element, the incorporation of an eigenvalue extraction method, plus the option to use structural displacements generated by the COUPLE [1] program when computing the acoustic pressure field.

In the discussion which follows, details concerning the development and incorporation of these latest enhancements to the AVAST suite will be presented.

2. DEVELOPMENT OF A FOUR-NODED ACOUSTIC PANEL ELEMENT

2.1 Introduction

In Phases I and II of this work [2,3] solution techniques based on a three-noded constant pressure fluid panel and an eight-noded isoparametric fluid element were developed and implemented in the AVAST suite. Unfortunately neither fluid element preserves compatibility with the four-noded structural shell element found in the VAST element library [4]. As a result, a four-noded constant pressure acoustic fluid panel has been developed and incorporated into the latest version of the AVAST code.

In the following sections, a description of the mathematical formulation and numerical implementation of the new four-noded acoustic fluid panel will be presented. This will be followed by a series of numerical trials which will demonstrate the reliability of this latest addition to AVAST fluid element library.

2.2 Boundary Integral Equation Formulation

The boundary integral formulation governing the response of an exterior acoustic fluid, bounded by a surface S, is provided below in Equation (2.1),

$$\{M_k \psi\}(p) = \left\{L_k \frac{\partial \psi}{\partial n}\right\}(p) \tag{2.1}$$

where ψ represents the acoustic pressure, k represents the acoustic wavenumber, n represents the outward normal to the surface S, p represents a point on the surface S and M_k and L_k denote integral operators, which may be defined as:

$$\{L_k \mu\}(p) = \int_S G_k(p,q)\, \mu(q)\, dS_q \tag{2.2}$$

$$\{M_k \mu\}(p) = \int_S \frac{\partial G_k}{\partial n_q}(p,q)\, \mu(q)\, dS_q \tag{2.3}$$

where in Equations (2.2) and (2.3) n_q is the unit outward normal to the surface S at a point q, $\mu(q)$ is a bounded function defined for q on S [5], and $G_k(p,q)$ is the Green's function which satisfies the Helmholtz equation (5), which in the case of an infinite three-dimensional fluid domain, has the form provided in Equation (2.4),

$$G_k(p,q) = \frac{e^{ikr_{pq}}}{4\pi r_{pq}} \tag{2.4}$$

where r_{pq} represents the distance between the two points p and q.

2.3 Numerical Implementation of the Boundary Integral Method Using Collocation

The numerical implementation of the boundary integral equation method, commonly referred to as the boundary element method, is derived by replacing the surface S by an approximate surface and the bounding functions by a linear combination of basis functions [6]. The symbol $\tilde{S}$ is used to represent the approximate surface and can be written as the sum of a series of m four-noded boundary elements or panels,

$$\tilde{S} = \sum_{j=1}^{m} \Delta\tilde{S}_j \tag{2.5}$$

where $\Delta\tilde{S}_j$ represents the portion of the original surface S discretized by the j-th four-noded quadrilateral boundary element. Having now replaced S with $\tilde{S}$, the boundary function $\mu(q)$ may be replaced by $\tilde{\mu}(q)$, and the integral operators L_k and M_k may be replaced by the operators $\tilde{L}_k$ and $\tilde{M}_k$ with respect to the approximate boundary $\tilde{S}$,

$$\left\{\tilde{L}_k\tilde{\mu}\right\}(p) = \int_{\tilde{S}} G_k(p,q)\,\tilde{\mu}(q)\,dS_q \tag{2.6}$$

$$\left\{\tilde{M}_k\tilde{\mu}\right\}(p) = \int_{\tilde{S}} \frac{\partial G}{n_q}(p,q)\,\tilde{\mu}(q)\,dS_q \tag{2.7}$$

Collocation of the boundary function $\tilde{\mu}(q)$ then permits the definition of a discrete form of $\{\tilde{L}_k\tilde{\mu}\}(p)$ and $\{\tilde{M}_k\tilde{\mu}\}(p)$. Let $P_1, P_2,\ldots,P_m$ be the m collocation points and let $\tilde{\chi}_1,\tilde{\chi}_2,\ldots,\tilde{\chi}_m$ be basic functions having the properties,

$$\tilde{\chi}_i(P_j) = \begin{cases} 1 & when \quad i=j \\ 0 & when \quad i\neq j \end{cases} \tag{2.8}$$

$$\sum_{j=1}^{m} \tilde{\chi}_j(q) = 1 \quad for\ q\ on\ S \tag{2.9}$$

The boundary function $\tilde{\mu}(q)$ may then be approximated as follows,

$$\tilde{\mu}(q) \simeq \sum_{j=1}^{m} \tilde{\mu}(P_j)\tilde{\chi}_j(q) \quad for\ q\ on\ S \tag{2.10}$$

The substitution of the approximation given above in Equation (2.10) into the definitions for the integral operators (Equations (2.6) and (2.7)) allows for their expression in discrete form,

$$\{\tilde{L}_k\tilde{\mu}\}(p) \simeq \sum_{j=1}^{m}\left[\tilde{\mu}(P_j)\{\tilde{L}_k\tilde{\chi}_j\}(p)\right] \tag{2.11}$$

$$\{\tilde{M}_k\tilde{\mu}\}(p) \simeq \sum_{j=1}^{m}\left[\tilde{\mu}(P_j)\{\tilde{L}_k\tilde{\chi}_j\}(p)\right] \tag{2.12}$$

The discrete operators may also be written in more familiar matrix notation,

$$[L_k]_{ij} = \{\tilde{L}_k\tilde{\chi}_j\}(P_i) \tag{2.13}$$

$$[M_k]_{ij} = \{\tilde{M}_k\tilde{\chi}_j\}(P_i) \tag{2.14}$$

where L_k and μ_k are m by m matrices. Substitution of Equations (2.13) and (2.14) into Equation (2.1) then yields the boundary element formulation of the exterior acoustic radiation problem, given below in Equation (2.15),

$$[M_k]\underline{\Psi} = [L_k]\underline{\mu} \tag{2.15}$$

where

$$\underline{\Psi} = [\psi(P_1),\ \psi(P_2),\ldots,\psi(P_m)]^T$$

$$\underline{\mu} = \left[\frac{\partial\psi}{\partial n}(P_1),\ \frac{\partial\psi}{\partial n},\ldots,\frac{\partial\psi}{\partial n}(P_m)\right]^T$$

2.4 Numerical Evaluation of the Discrete Forms Using a Four-Noded Boundary Element

When the fluid boundary S is discretized into small, four-noded quadrilateral panel elements, the acoustic pressure (ψ) and pressure gradients $\left(\frac{\partial\psi}{\partial n}\right)$ are assumed to be constant over each element. This leads to the following forms for the matrix components,

$$[M_k]ij = \iint_{\Delta\bar{S}_j} \frac{\partial}{\partial n_j}\left(G_k(P_i,q_j)\right)\, ds_j = \iint_{\Delta\bar{S}_j} \frac{\partial}{\partial n}\left(\frac{e^{-ikr(P_i,q_j)}}{r(P_i,q_j)}\right) ds_j \tag{2.16}$$

$$[L_k]ij = \iint_{\Delta\bar{S}_j} \left(G_k(P_i,q_j)\right)\, ds_j = \iint_{\Delta\bar{S}_j} \left(\frac{e^{-ikr(P_i,q_j)}}{r(P_i,q_j)}\right) ds_j \tag{2.17}$$

Before evaluating the integrals provided above, the four-noded quadrilateral element is first projected onto a plane passing through its centroid, as shown in Figure 2.1. By doing so, a single unique value for the surface normal is imposed over the element [7]. Once this has been completed, the projected surface is mapping into a ϵ-η two-dimensional space using the following shape functions,

$$P(\epsilon,\eta) = \sum_{l-1}^{4} N_l(\epsilon,\eta) \tag{2.18}$$

where

$$\left.\begin{aligned} N_1(\epsilon,\eta) &= \frac{1}{4}(1-\epsilon)(1-\eta) \\ N_2(\epsilon,\eta) &= \frac{1}{4}(1+\epsilon)(1-\eta) \\ N_3(\epsilon,\eta) &= \frac{1}{4}(1-\epsilon)(1+\eta) \\ N_4(\epsilon,\eta) &= \frac{1}{4}(1-\epsilon)(1-\eta) \end{aligned}\right\} \qquad (2.19)$$

Gaussian numerical integration is then used to evaluate the matrix coefficients given in Equations (2.16) and (2.17). For cases where the points p and q reside on the same panel, special techniques are used to extract the resulting singularity from the integral kernel. These singular terms are evaluated separately before being re-combined with the regular term. These singularity handling techniques are well documented in the literature [8].

2.5 Numerical Example

In order to verify the accuracy of the new four-noded acoustic panel, the sound radiated from a uniformly pulsating sphere was modelled and compared to its exact analytical solution [8] (as shown in Figure 2.2). Although challenging, the four-noded panel was able to model the spherical geometry extremely well.

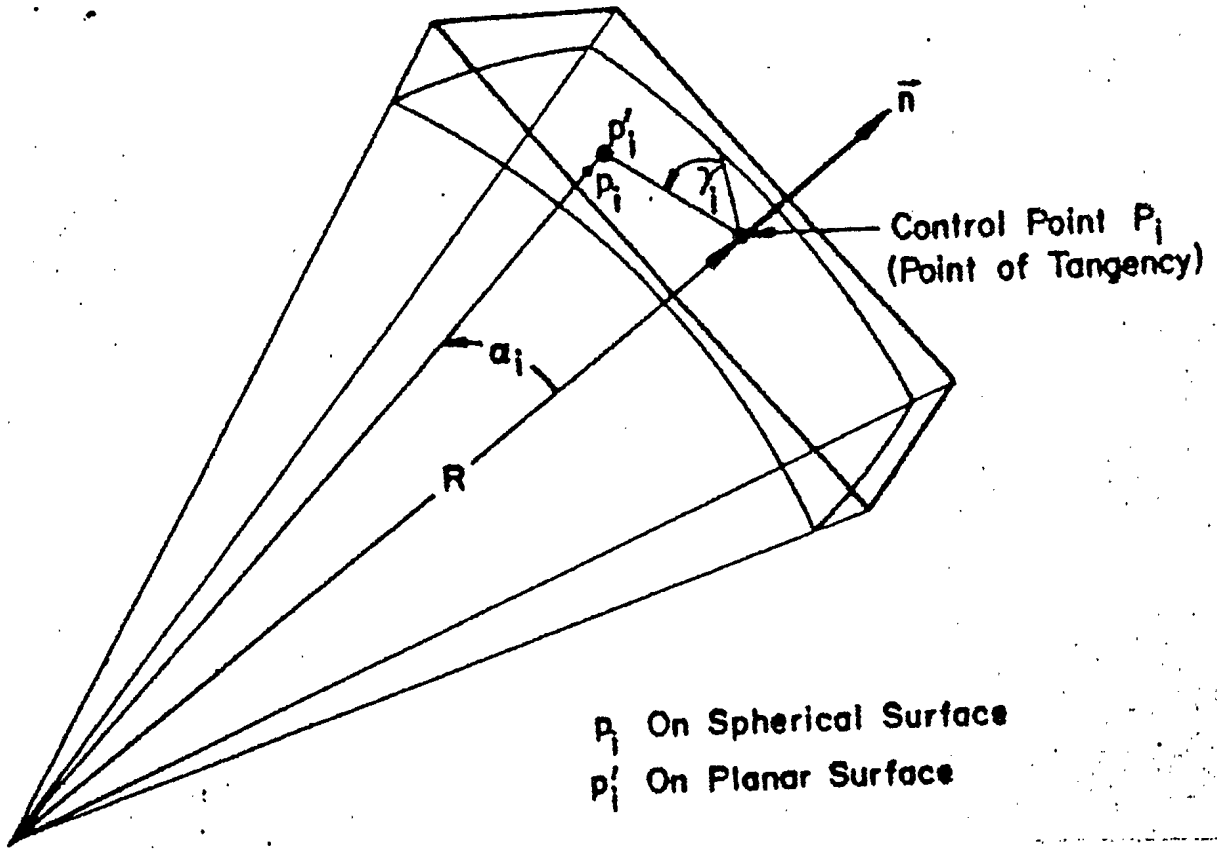

FIGURE 2.1: Quadrilaterial Panel Projection
(Reproduced From [7])

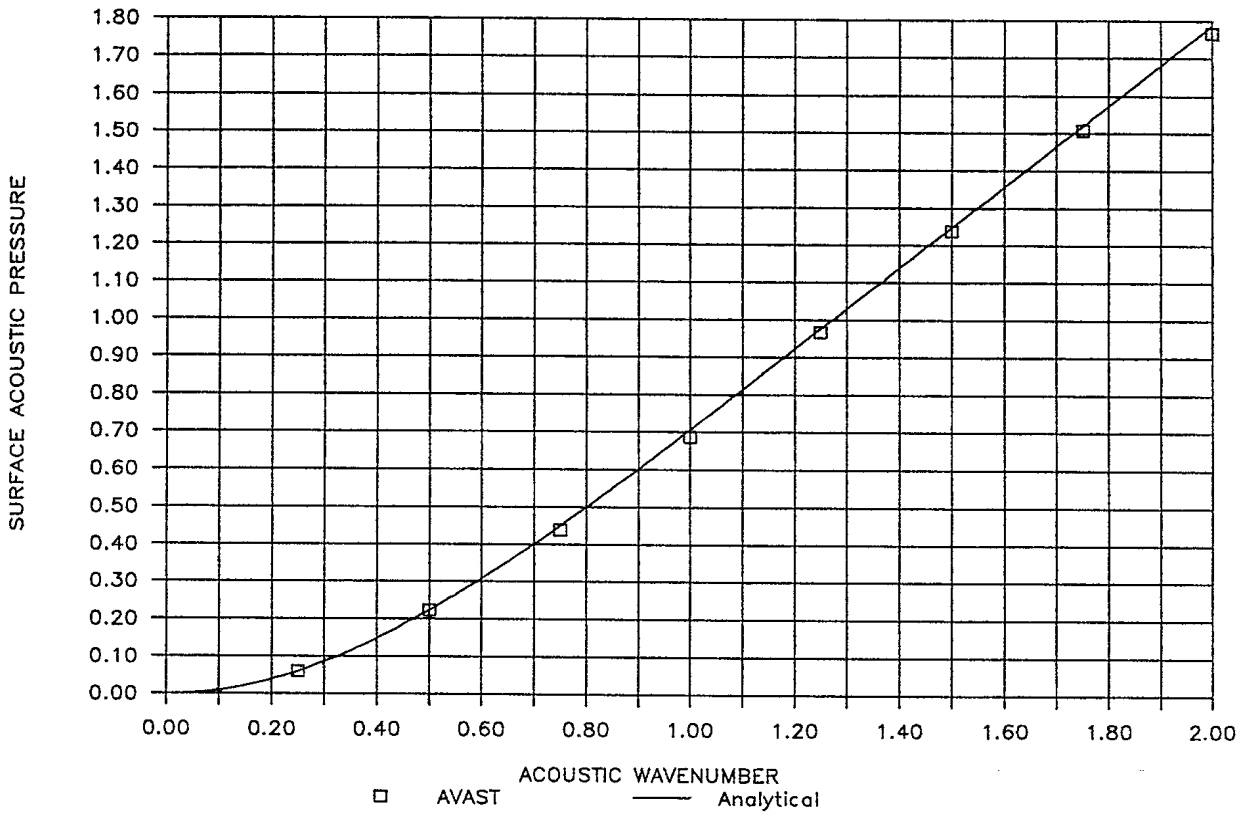

FIGURE 2.2: Surface Pressures Generated by a Uniformly Vibrating Spherical Shell of Radius 1.0 Modelled Using a Four-Noded Surface Panel Element

3. MODAL ANALYSIS OF ACOUSTICALLY LOADED STRUCTURES VIA INTEGRAL EQUATION METHODS

3.1 Introduction

In this chapter, the problem of computing the frequency response and natural frequencies of a linear elastic structure in contact with an acoustic medium is considered. This work was prompted by a recent study [9] which reviewed a number of numerical methods commonly used to predict radiated noise generated by submerged elastic structures. These methods (including both finite element and integral equation methods) differed most significantly in the approach adopted for modelling both the structural response and fluid/structure coupling. In order to evaluate the performance of the different numerical schemes, numerical predictions were compared to both analytical results and experimentally measured values. These tests showed that methods which exploit the eigenvalues and associated eigenmodes of the "wet" structure provide a more accurate picture of the radiated noise patterns than do other techniques. This was especially true when the structure was loaded at a resonant frequency.

In light of these recent findings, and due to interest in modelling the acoustic response of submerged structures excited at the coupled fluid/structure natural frequencies, it has been proposed that a eigenvalue extraction technique be incorporated into an upgraded version of the AVAST code. In the sections which follow, a method capable of computing the natural frequencies of the complex, nonsymmetric and frequency dependent matrices resulting from the coupling of the equations governing the fluid and structural responses will be described. This will be followed by a number of examples which will demonstrate the utility of this new technique.

3.2 Solution of the Helmholtz Eigenvalue Problem Via the Boundary Element Method

In this section, a computational method for solving the Helmholtz eigenvalue problem, based to a large degree on the work of Stephen Kirkup [10,11], is described. The problem is that of finding the values of the acoustic wavenumber k and a nontrivial scalar function ψ such that the Helmholtz equation,

$$\nabla^2\psi(p) + k^2\psi(p) = 0 \tag{3.1}$$

is satisfied in a fluid domain D with boundary S and subject to a homogeneous boundary condition of the form,

$$a(p)\,\psi(p) + b(p)\frac{\partial}{\partial n_p}\psi(p) = 0 \tag{3.2}$$

where $a(p)$ and $b(p)$ are known complex-valued functions of p and n_p is the unit outward normal to the boundary at p. According to Kirkup [11], the nontrivial solutions $k=k^*$ and $\psi(p) = \psi^*(p)$ are termed the eigenfrequencies and eigenfunctions, and they are dependent on the boundary S and the boundary functions $a(p)$ and $b(p)$. It is also important to note that the eigenfrequencies are all expected to be real numbers or complex numbers having relatively small imaginary components.

The Helmholtz eigenvalue problem is amenable to solution via a number of techniques, including both the finite difference and finite element methods. In these cases, the problem reduces to that of solving a generalized linear eigenvalue problem of the form,

$$(A - k^2 B)\underline{x} = \underline{0} \tag{3.3}$$

Given the special structure of the matrices and the fact that a variety of standardized solution techniques are available, the eigenfrequency analysis of the Helmholtz problem via the finite element or finite difference method is straightforward. In contrast, the application of the boundary element method reduces the Helmholtz eigenvalue problem to that of solving an eigenvalue problem of the form,

$$A_k\underline{\mu} = \underline{0} \tag{3.4}$$

where the matrix A_k is fully populated, with each component being a continuously differentiable complex-valued function of k [11].

3.2.1 Literature Review

The problem of solving the Helmholtz eigenvalue problem via boundary element-type methods has been given some consideration by researchers. One of the earliest known papers published on this topic is attributed to Banerjee, Ahmad and Wang [12]. Their formulation was based on the method of constructing a solution of a differential equation in terms of a complementary function and particular

integral. This leads to a system of equations similar to that given in Equation (3.3), which could then be solved using a block iteration algorithm similar to that found in the EISPACK library [13]. Coyette and Fyfe [14], in a subsequent study, applied a subspace iteration scheme to the method of Banerjee, et al., which, according to the authors, greatly enhanced the calculation speed. More recently, Rajakumar and Ali [15] used the method of Banerjee et al. to compute the modal characteristics of acoustical cavities having sound absorptive characteristics. In this work, the acoustic boundary element eigenproblem was first set up as shown by Banerjee [12], then a simple method of incorporating the boundary absorption into the boundary element formulation was then described. Finally, the resulting quadratic eigenvalue problem was solved using the Lanczos algorithm.

An alternative to the techniques described above was recently published by Kirkup and Amini [11]. In their paper, they describe a method which approximates each component of the matrix A_k by a polynomial in k over some subrange of the full wavenumber range. This permitted the reformulation of the nonlinear eigenvalue problem, given in Equation (3.4), in the form of a standard generalized eigenvalue problem. As a result, all the eigenvalues in the subrange could be computed simultaneously. The method was applied to the axisymmetric three-dimensional problem where the surface was a sphere. The effectiveness of the method was studied through considering the results of varying the width of the wavenumber subrange, the number of boundary elements and the degree of the interpolating polynomial.

3.2.2 Recommendations Based on Literature Review

After reviewing the numerical procedures outlined in the literature, the method of Kirkup and Amini [11] appears to be the most suitable for implementation in the current AVAST program. The other techniques, based largely on the work of Banerjee et al., are not well suited for problems which may include nonzero surface velocity boundary conditions, which is of great interest to users of the AVAST suite.

3.3 A Review of the Frequency Interpolation BEM Eigenvalue Extraction Technique

The first step in Kirkup's frequency interpolation technique is the selection of a wavenumber interval k_1-k_2, where $k_1 \le k \le k_2$. Next, the discrete forms $\left\{\tilde{L}_k \tilde{\chi}\right\}(p)$ and $\left\{\tilde{M}_k \tilde{\chi}\right\}(p)$ are evaluated at a set wavenumbers, γ, η, λ (see Equation 3.7) spanning the wavenumber interval. The number of interpolation wavenumbers depends on the order of the polynomial used to approximate the discrete

forms. At present, a quadratic interpolation scheme has been developed for AVAST. This leads to the following expressions for the discrete operators,

$$\left\{\tilde{L}_k\tilde{\chi}\right\}(p) \approx \left\{\tilde{L}_\gamma\tilde{\chi}\right\}(p) + \frac{1}{d}(k-\gamma)\left[\left\{\tilde{L}_\eta\tilde{\chi}\right\}(p) - \left\{\tilde{L}_\gamma\tilde{\chi}\right\}(p)\right] + \frac{1}{2d^2}(k-\gamma)(k-\eta)\left[\left\{\tilde{L}_\gamma\tilde{\chi}\right\}(p) - 2\left\{\tilde{L}_\eta\tilde{\chi}\right\}(p) + \left\{\tilde{L}_\lambda\tilde{\chi}\right\}(p)\right] \tag{3.5}$$

$$\left\{\tilde{M}_k\tilde{\chi}\right\}(p) \approx \left\{\tilde{M}_\gamma\tilde{\chi}\right\}(p) + \frac{1}{d}(k-\gamma)\left[\left\{\tilde{M}_\eta\tilde{\chi}\right\}(p) - \left\{\tilde{M}_\gamma\tilde{\chi}\right\}(p)\right] + \frac{1}{2d^2}(k-\gamma)(k-\eta)\left[\left\{\tilde{M}_\gamma\tilde{\chi}\right\}(p) - 2\left\{\tilde{M}_\eta\tilde{\chi}\right\}(p) + \left\{\tilde{M}_\lambda\tilde{\chi}\right\}(p)\right] \tag{3.6}$$

where:

$$\gamma = k_1 + \frac{1}{4}\left(2-\sqrt{3}\right)(k_2-k_1)$$

$$\eta = \frac{1}{2}\left(k_1+k_2\right)$$

$$\lambda = k_1 + \frac{1}{4}\left(2+\sqrt{3}\right)(k_2-k_1)$$

are the Chebychev quadratic interpolation points for the interval $[k_1,k_2]$ and

$$d = \eta-\gamma = \lambda-\eta = \frac{1}{4}(k_2-k_1)\sqrt{3} \tag{3.7}$$

The above forms of $\left\{\tilde{L}_k\tilde{\chi}\right\}(p)$ and $\left\{\tilde{M}_k\tilde{\chi}\right\}$ may be reduced to the following matrix forms,

$$\left\{\tilde{L}_k\tilde{\chi}_j\right\}(p_i) = [L_k]ij = [L_0]ij + k[L_1]ij + k^2[L_2]ij \tag{3.8}$$

$$\left\{\tilde{M}_k\tilde{\chi}_j\right\}(p_i) = [M_k]ij = [M_0]ij + k[M_1]ij + k^2[M_2]ij \tag{3.9}$$

where

$$[L_0]ij = \{\tilde{L}_\gamma \tilde{\chi}_j\}(p_i) - \frac{\gamma}{d}\left[\{\tilde{L}_\eta \tilde{\chi}_j\}(p_i) - \{\tilde{L}_\gamma \tilde{\chi}_j\}(p_i)\right] + \frac{\gamma\eta}{2d^2}\left[\{\tilde{L}_\gamma \tilde{\chi}_j\}(p_i) - 2\{\tilde{L}_\eta \tilde{\chi}_j\}(p_i) + \{\tilde{L}_\gamma \tilde{\chi}_j\}(p_i)\right] \quad (3.10)$$

$$[L_1]ij = \frac{1}{d}\left[\{\tilde{L}_\eta \tilde{\chi}_j\}(p_i) - \{\tilde{L}_\gamma \tilde{\chi}_j\}(p_i)\right] - \frac{(\eta+\gamma)}{2d^2}\left[\{\tilde{L}_\gamma \tilde{\chi}_j\}(p_i) - 2\{\tilde{L}_\eta \tilde{\chi}_j\}(p_i) + \{\tilde{L}_\gamma \tilde{\chi}_j\}(p_i)\right] \quad (3.11)$$

$$[L_2]ij = \frac{1}{2d^2}\left[\{\tilde{L}_\gamma \tilde{\chi}_j\}(p_i) - 2\{\tilde{L}_\eta \tilde{\chi}_j\}(p_i) + \{\tilde{L}_\lambda \tilde{\chi}_j\}(p_i)\right] \quad (3.12)$$

$$[M_0]ij = \{\tilde{M}_\gamma \tilde{\chi}_j\}(p_i) - \frac{\gamma}{d}\left[\{\tilde{M}_\eta \tilde{\chi}_j\}(p_i) - \{\tilde{M}_\gamma \tilde{\chi}_j\}(p_i)\right] + \frac{\gamma\eta}{2d^2}\left[\{\tilde{M}_\gamma \tilde{\chi}_j\}(p_i) - 2\{\tilde{M}_\eta \tilde{\chi}_j\}(p_i) + \{\tilde{M}_\gamma \tilde{\chi}_j\}(p_i)\right] \quad (3.13)$$

$$[M_1]ij = \frac{1}{d}\left[\{\tilde{M}_\eta \tilde{\chi}_j\}(p_i) - \{\tilde{M}_\gamma \tilde{\chi}_j\}(p_i)\right] - \frac{(\eta+\gamma)}{2d^2}\left[\{\tilde{M}_\gamma \tilde{\chi}_j\}(p_i) - 2\{\tilde{M}_\eta \tilde{\chi}_j\}(p_i) + \{\tilde{M}_\gamma \tilde{\chi}_j\}(p_i)\right] \quad (3.14)$$

$$[M_2]ij = \frac{1}{2d^2}\left[\{\tilde{M}_\gamma \tilde{\chi}_j\}(p_i) - 2\{\tilde{M}_\eta \tilde{\chi}_j\}(p_i) + \{\tilde{M}_\lambda \tilde{\chi}_j\}(p_i)\right] \quad (3.15)$$

with the discrete forms of the integral operators given in Equations (3.8) and (3.9), the following relationship between acoustic pressure and its gradient with respect to the surface normal can be generated,

$$\left([L_0]+k[L_1]+k^2[L_2]\right)\underline{u} = \left([M_0]+k[M_1]+k^2[M_2]\right)\underline{\psi} \quad (3.16)$$

where:

$\underline{\psi}$ represents the vector of acoustic pressures

$\underline{u}$ represents the vector of $\frac{\partial \psi}{\partial n}$

With the Helmholtz equation now in the form provided above in Equation (3.16), the nonlinear eigenvalue problem described by Equation (3.4) can be replaced with the following eigenvalue problem:

$$\left([A_0]+k[A_1]+k^2[A_2]\right)\underline{\mu} = \underline{0} \tag{3.17}$$

with the solution of Equation (3.17) being the same as those of the following generalized linear eigenvalue problem,

$$\begin{bmatrix}[A_0] & [A_1]\\ 0 & [I]\end{bmatrix}\begin{Bmatrix}\underline{\mu}\\ k\underline{\mu}\end{Bmatrix} = k\begin{bmatrix}0 & -[A_2]\\ [I] & 0\end{bmatrix}\begin{Bmatrix}\underline{\mu}\\ k\underline{\mu}\end{Bmatrix} \tag{3.18}$$

3.4 Verification of the Frequency Interpolation BEM Eigenvalue Extraction Technique

In order to verify that the frequency interpolation scheme (FIS) proposed by Kirkup would be appropriate for use with the AVAST suite, a computer program based on the FIS was developed and the output compared to data published in a similar study [11]. The solver used to compute the eigenfrequencies of the assembled matrix given in Equation (3.18) was the ZGEGV LAPACK [16] routine, which is based on the QZ algorithm [17].

The verification tests involved calculating the Dirichlet $(\underline{\mu} = \underline{0})$ and Neumann$(\underline{\psi} = 0)$ eigenfrequencies of a sphere having a radius of 1.0. For the Dirichlet problem the generalized eigenvalue problem has the following form,

$$\begin{bmatrix}[L_0] & [L_1]\\ 0 & [I]\end{bmatrix}\begin{Bmatrix}\underline{\psi}\\ k\underline{\psi}\end{Bmatrix} = k\begin{bmatrix}0 & -[L_2]\\ [I] & 0\end{bmatrix}\begin{Bmatrix}\underline{\psi}\\ k\underline{\psi}\end{Bmatrix} \tag{3.19}$$

whereas the equation related to the Neumann eigenvalue problem has the following form,

$$\begin{bmatrix}[M_0] & [M_1]\\ 0 & [I]\end{bmatrix}\begin{Bmatrix}\underline{\mu}\\ k\underline{\mu}\end{Bmatrix} = k\begin{bmatrix}0 & -[M_2]\\ [I] & 0\end{bmatrix}\begin{Bmatrix}\underline{\mu}\\ k\underline{\mu}\end{Bmatrix} \tag{3.20}$$

The results from these tests, provided in Table 3.1 and Table 3.2, show excellent agreement with both data published by Kirkup [11] and analytical values, indicating that the FIS has significant potential as a method for computing eigenvalues of matrices generated by the boundary integral equation method.

3.5 Estimating Coupled Fluid/Structure Natural Frequencies Using the Frequency Interpolation Method

The coupling of the governing finite element based structural equation and the boundary element based fluid equation leads to the following nonlinear eigenvalue problem,

$$\left([K] + i\omega[C] - \omega^2[M_s] - \rho\omega^2[T]^T[A][M_\omega]^{-1}[L_\omega][T]\right)\underline{\delta} = \underline{0} \tag{3.21}$$

where:

[K]	represents the structural stiffness matrix
[C]	represents the structural damping matrix
$[M_s]$	represents the structural mass matrix
[T]	represents a transformation matrix between global cartesian coordinates and "wet" surface normal coordinates
[A]	represents the diagonal panel area matrix
$[M_\omega]$	represents the discrete form of the integral operator $\{M_\omega \mu\}$ (see Equation 2.3)
$[L_\omega]$	represents the discrete form of the integral operator $\{L_\omega \mu\}$ (see Equation 2.2)
ρ	represents the fluid density
ω	represents the driving frequency
$\underline{\delta}$	represents the vector of nodal structural displacements

Equation (3.21) can be replaced, however, with the following restatement of the eigenvalue problem:

$$\left[[K] + i\omega[C] - \omega^2\left([M_s] + [Ma_1] + \omega[Ma_2] + \omega^2[Ma_1]\right)\right]\underline{\delta} = \underline{0} \tag{3.22}$$

where the matrices $[Ma_1]$, $[Ma_2]$ and $[Ma_3]$ represent the frequency interpolated components of the "acoustic added mass" matrix $\rho[T]^T[A][M_\omega]^{-1}[L_\omega][T]$. In this form, the coupled eigenvalue problem can be solved using the same standard methods used to solve equations of the type given below,

$$\begin{bmatrix} [A_0] & [A_1] & [A_2] & [A_3] \\ 0 & [I] & 0 & 0 \\ 0 & 0 & [I] & 0 \\ 0 & 0 & 0 & [I] \end{bmatrix} \begin{bmatrix} \underline{\delta} \\ \omega\underline{\delta} \\ \omega^2\underline{\delta} \\ \omega^3\underline{\delta} \end{bmatrix} = \omega \begin{bmatrix} 0 & 0 & 0 & -[A_4] \\ [I] & 0 & 0 & 0 \\ 0 & [I] & 0 & 0 \\ 0 & 0 & [I] & 0 \end{bmatrix} \begin{bmatrix} \underline{\delta} \\ \omega\underline{\delta} \\ \omega^2\underline{\delta} \\ \omega^3\underline{\delta} \end{bmatrix} \tag{3.23}$$

where, for our purposes,

$[A_0] = [K]$

$[A_1] = i[C]$

$[A_2] = -[M_s] - [Ma_1]$

$$[A_3] = -[Ma_2]$$
$$[A_4] = -[Ma_3]$$

3.5.1 Wet Mode/Dry Mode Approach

Because of the significant computational requirements imposed by the direct solution of Equation (3.23), the decision was made to calculate the coupled, or wet, natural frequencies using a method based on the wet mode/dry mode algorithm employed in the VAST finite element code [4]. Essentially, this method uses the natural frequencies and mode shapes of the "dry" structure to transform Equation (3.22) into the following form,

$$i\omega[\Phi]^T[C][\Phi] - \omega^2[I] - \omega^2[\Phi]^T\left(\left[Ma_1\right] + \omega\left[Ma_2\right] + \omega^2\left[Ma_3\right]\right)[\Phi]\Big). \tag{3.24}$$

where:

$[\Phi]$ represents a matrix whose columns are the dry structural mode shapes orthogonalized with respect to the structural mass matrix

ω_i represents the i-th natural frequency of the dry structure

$$[\Omega]_{ij} = \begin{cases} 0 & i \neq j \\ \omega_i^2 & i = j \end{cases}$$

$\underline{u}$ represents a vector of generalized displacements, where $[\Phi]\underline{u} = \underline{\delta}$

A computer program, based on this wet mode/dry mode approach, has been developed and recently incorporated into an upgraded version of the AVAST code. Preliminary testing indicates that this method is a highly effective tool for the prediction of coupled fluid/structure natural frequencies.

3.6 AVAST Frequency Response Capability

With the successful development of the eigenvalue extraction technique, it was decided to add a frequency response capability to the current AVAST program. Such a feature would allow users to compute the response of the "wet" structure using the modal characteristics of the dry structure. The governing equation for the frequency response of the coupled fluid/structure system has the form given below in Equation (3.25),

$$\left([K] - \omega^2[M_s + M_a(\omega)] + i\omega[C]\right)\underline{\delta} = f \tag{3.25}$$

where $[M_a(\omega)]$ is the frequency dependent acoustic added mass matrix and f represents a vector of structural nodal forces.

By adopting the mode shapes and natural frequencies of the dry structure, the governing equation of motion for the coupled system can be converted into a generalized coordinate system having the form,

$$\left([\Omega] - \omega^2[I] - \omega^2[\Phi]^T[M_a(\omega)][\Phi] + i\omega[\Phi]^T[C][\Phi]\right)\underline{u} = \underline{q} \tag{3.26}$$

where $\underline{q}$ represents the applied structural load transformed into the generalized coordinate system. Equation (3.26) can be simplified by restricting the structural damping to have the following form,

$$[C] = \alpha_k[K] + \alpha_m[M_s] \tag{3.27}$$

Substituting Equation (3.27) into (3.26) then yields,

$$\left(\left(1 + i\omega\alpha_k\right)[\Omega] - \omega^2\left(1 - \frac{i\alpha_m}{\omega}\right)[I] - \omega^2[\Phi]^T[M_a(\omega)][\Phi]\right)\underline{u} = \underline{q} \tag{3.28}$$

Solving for the generalized displacements using Equation (3.28) then yields the following expression,

$$\underline{u} = [A]\,\underline{q} \tag{3.29}$$

where the matrix [A] may be defined as,

$$[A] = \left[\left(1 + i\omega\alpha_k\right)[\Omega] - \omega^2\left(1 - \frac{i\alpha_m}{\omega}\right)[I] - \omega^2[\Phi]^T[Ma(\omega)][\Phi]\right]^{-1} \tag{3.30}$$

3.6.1 Validation of the AVAST Frequency Response Feature

In order to verify that the results generated by the AVAST frequency response algorithm were reasonable, a series of numerical trials were performed using two models representing DREA's acoustic test cylinder. A detailed description of the acoustic cylinder is provided in Reference [19]. The first model (CYLN1), shown here in Figure 3.1, is similar to the actual physical cylinder in most respects,

except that it is modelled without endcaps and stiffeners. Omitting these features was justified on the basis of model size reduction and solution speed. In addition, model CYLN1 had the translational degrees-of-freedom fixed at both ends (a situation not found in the physical model tests). A second model was also developed for this study (CYLN2). This model being identical to CYLN1, except that all boundary conditions were omitted. Both models were loaded using a single point load, having a magnitude of 10N, acting radially outward and located at a point positioned on the mid-plane of the cylinder (see Figure 3.1). Field pressures were then computed for a number of points forming a "ring" surrounding the cylinder (see Figure 3.2).

Figures 3.3 through 3.8 provide polar plots of the acoustic field pressures produced by the CYLN1 model when loaded at frequencies corresponding to the first six "wet" natural modes of the constrained structure. The deformed shapes corresponding to these nodes are provided in Figures 3.15 through 3.20, respectively. Figures 3.9 through 3.14 provide polar plots of the acoustic field pressures produced by the CYLN2 model when loaded at frequencies corresponding to the first six "wet" natural modes of the "free-free" structure. The deformed shapes corresponding to these modes are provided in Figures 3.21 through 3.25, respectively.

A comparison of Figures 3.3 through 3.14 with similar results produced by the actual test cylinder does seem to indicate that the algorithms now found in the AVAST code are capable of predicting the sound pressure levels and acoustic signatures of submerged elastic structures.

TABLE 3.1: Computed Dirichlet Eigenfrequencies			
Mode #	Analytical Value	Kirkup [11]	Martec
1	3.14159	3.142+i0.00051	3.147+i0.00083
2	4.49341	4.49002+i0.00029	4.557+i0.00042
3	5.76346	5.7575-i0.000422	5.842-i0.0001
4	6.28319	6.27428-i0.00055	6.46-i0.00038

TABLE 3.2: Computed Neumann Eigenfrequencies			
Mode #	Analytical Value	Kirkup [11]	Martec
1	3.14159	3.344+i0.0156	3.156+i0.0004

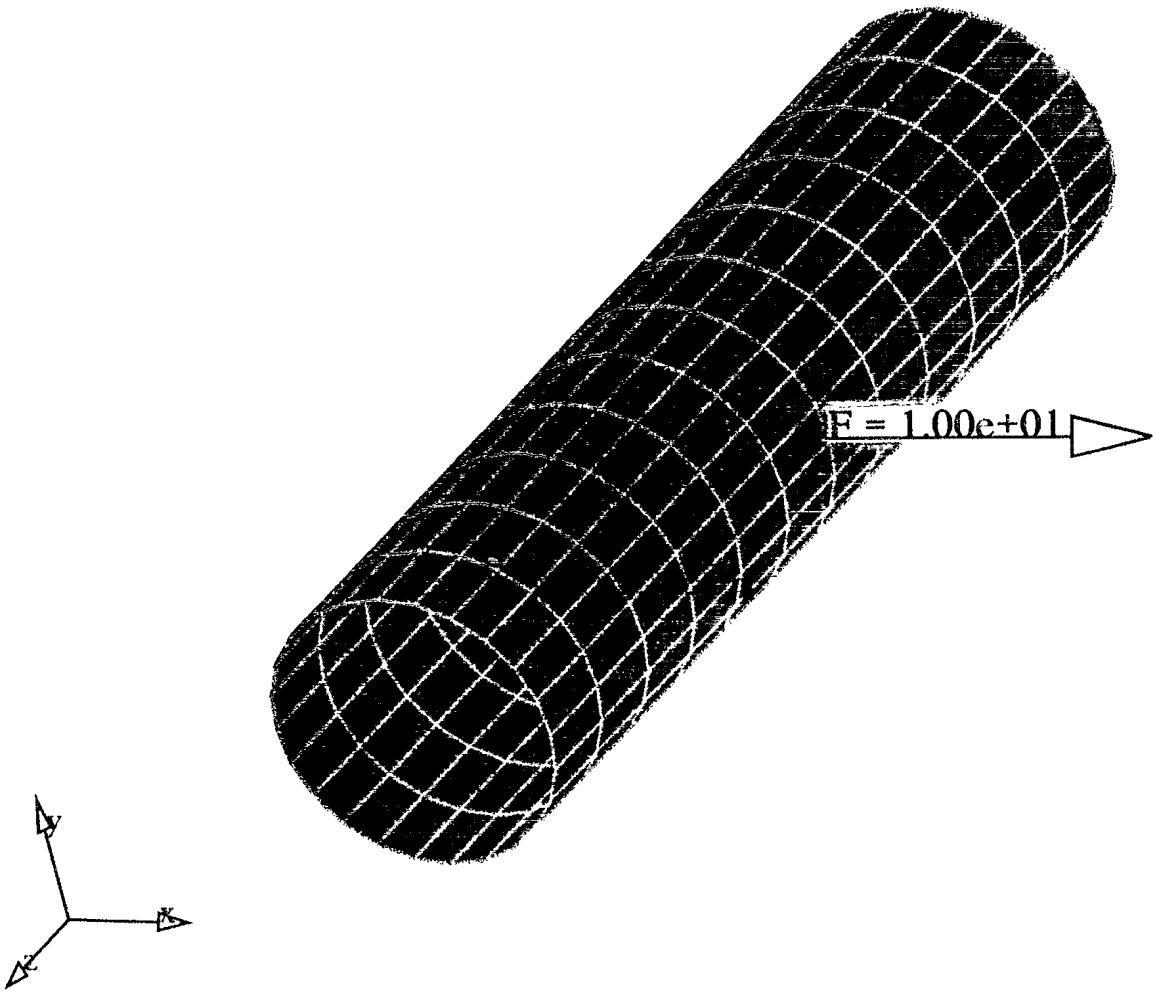

FIGURE 3.1: Finite Element Model of the CYLN2 Model
(Position of the Load is Marked With the Label "F")

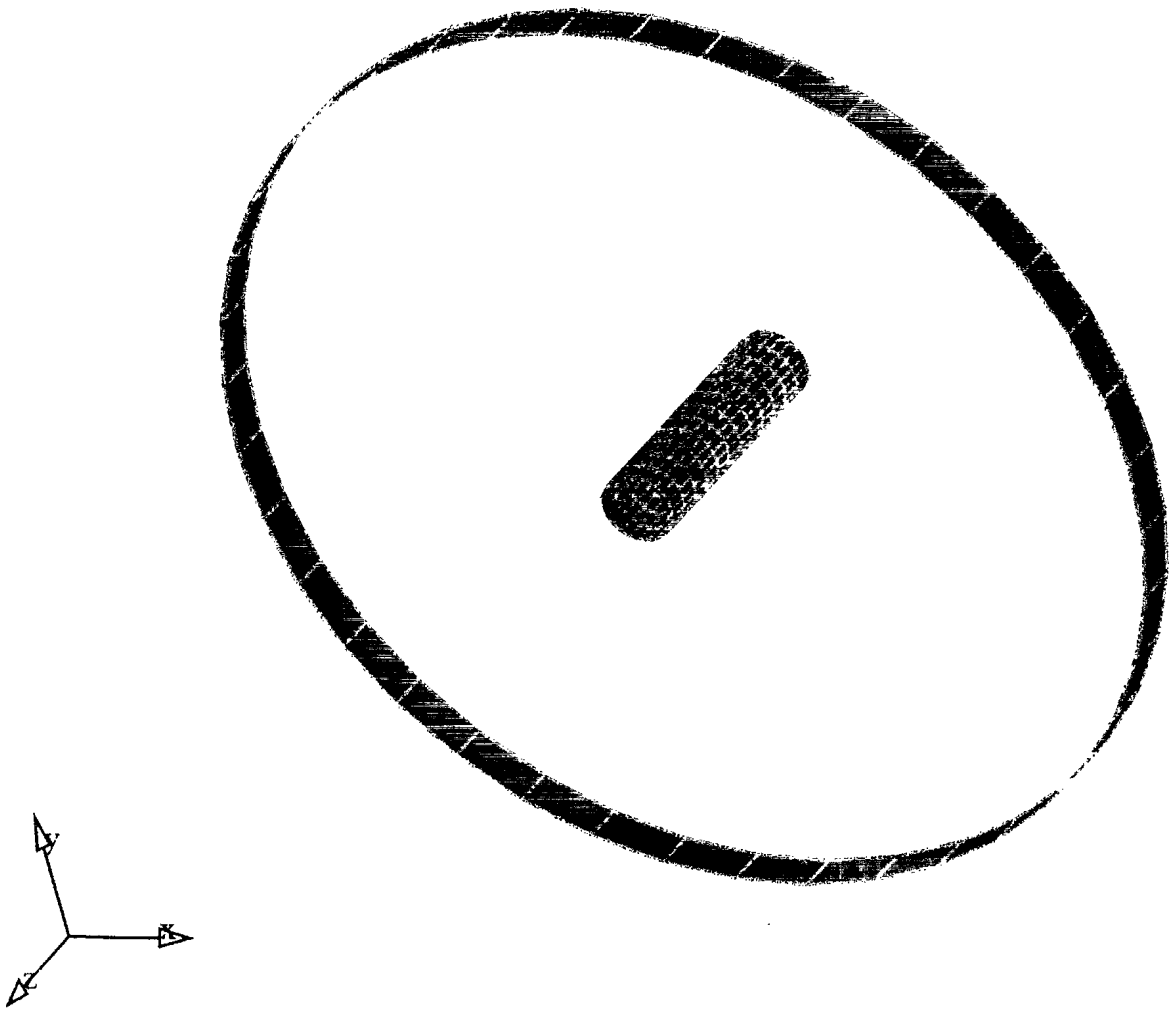

FIGURE 3.2: Ring of Field Point Locations (in blue) Surrounding the Mid-Plane of the Cylinder

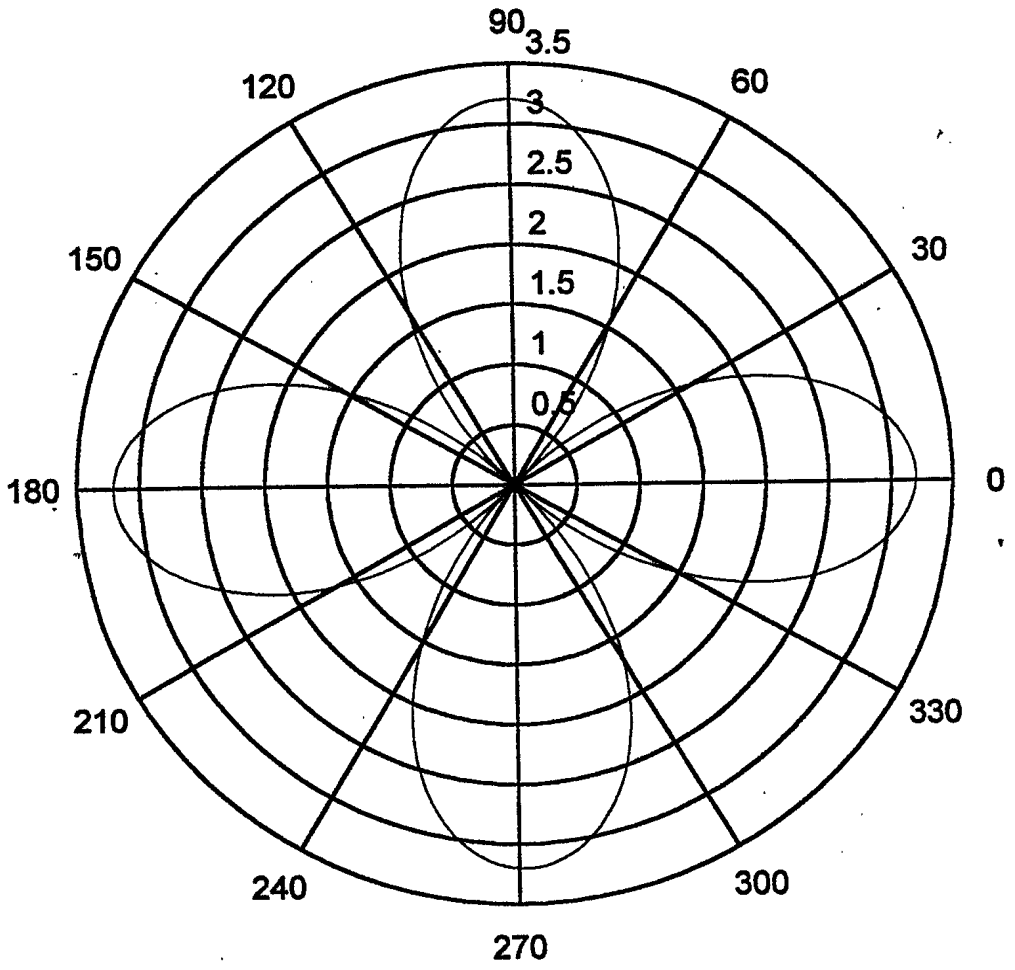

FIGURE 3.3: Field Pressures Produced by the CYLN1 Model Vibrating at the First Coupled Natural Frequency

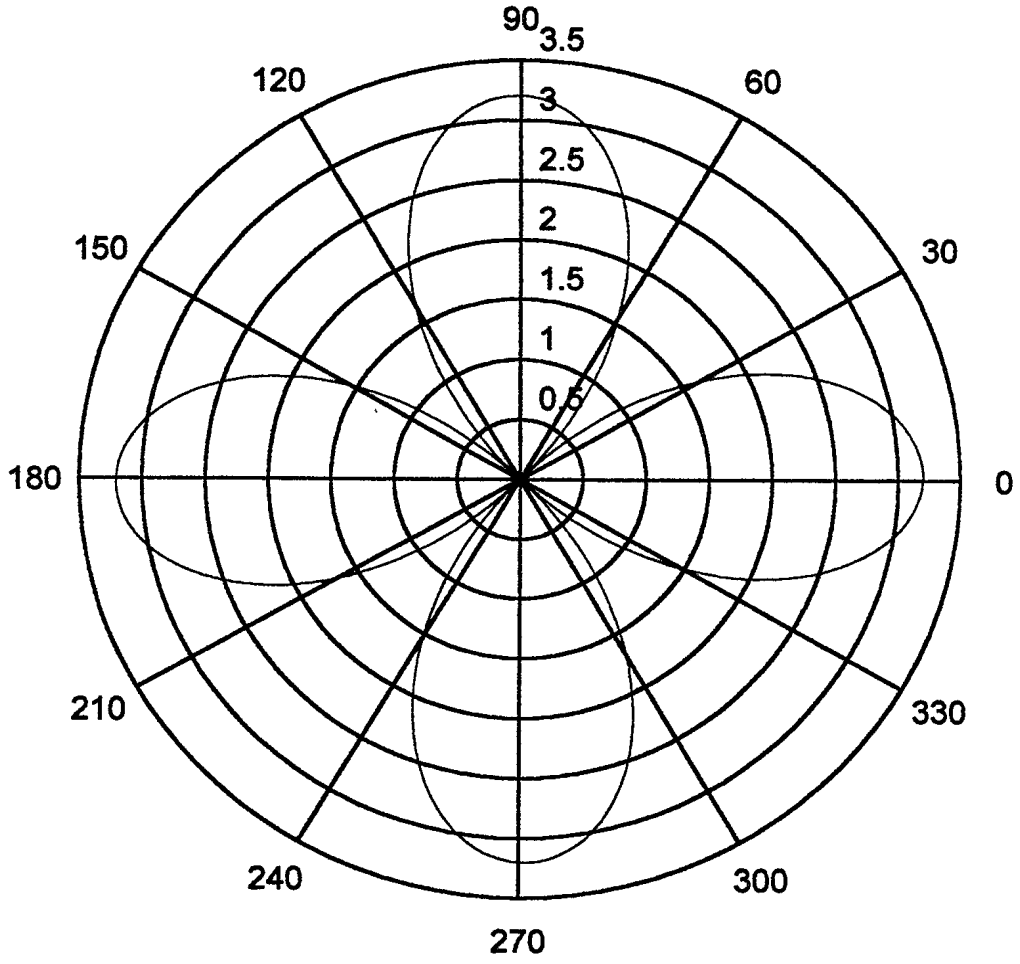

FIGURE 3.4: Field Pressures Produced by the CYLN1 Model Vibrating at the Second Coupled Natural Frequency

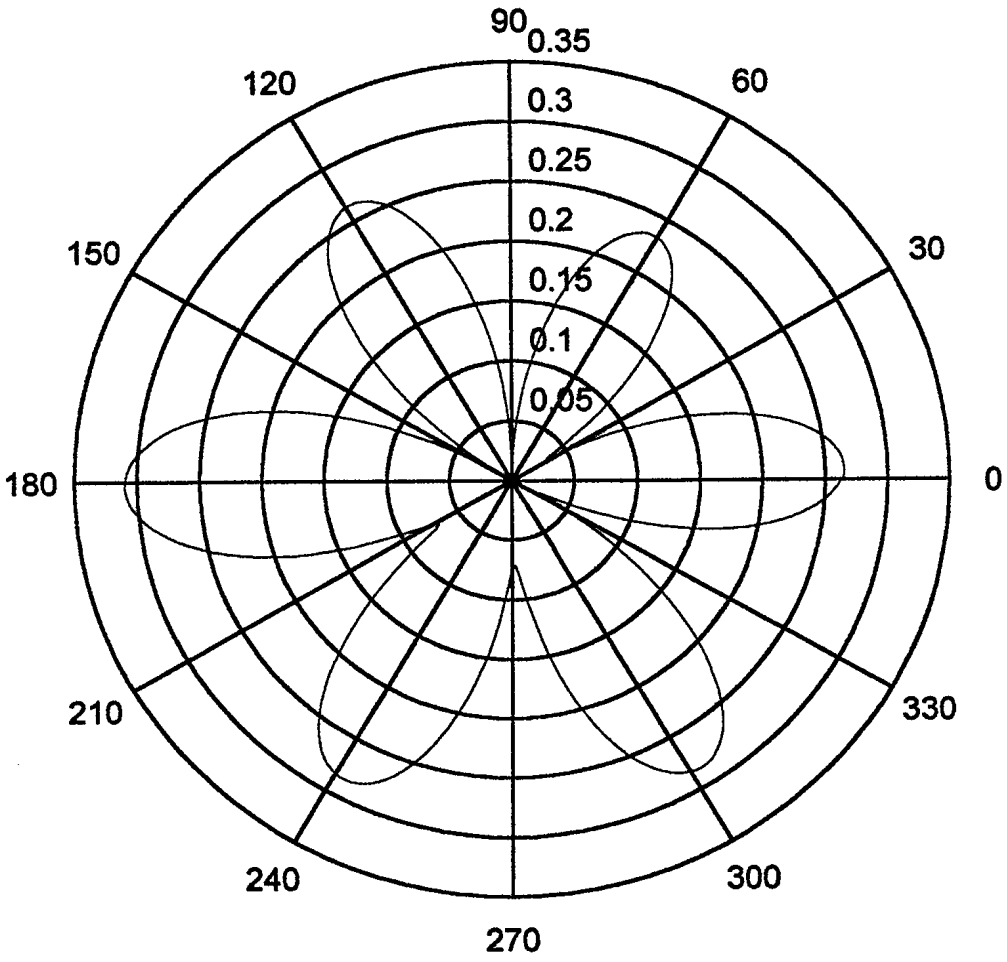

FIGURE 3.5: Field Pressures Produced by the CYLN1 Model Vibrating at the Third Coupled Natural Frequency

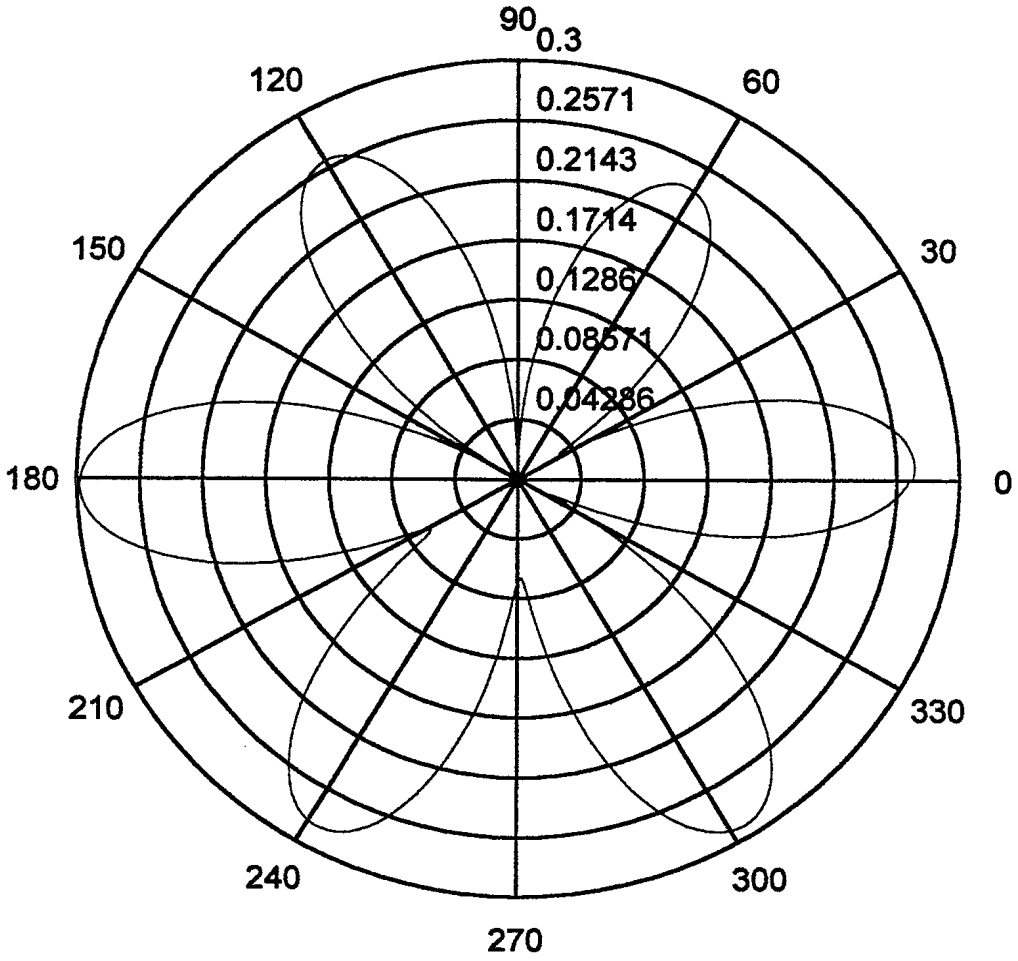

FIGURE 3.6: Field Pressures Produced by the CYLN1 Model Vibrating at the Fourth Coupled Natural Frequency

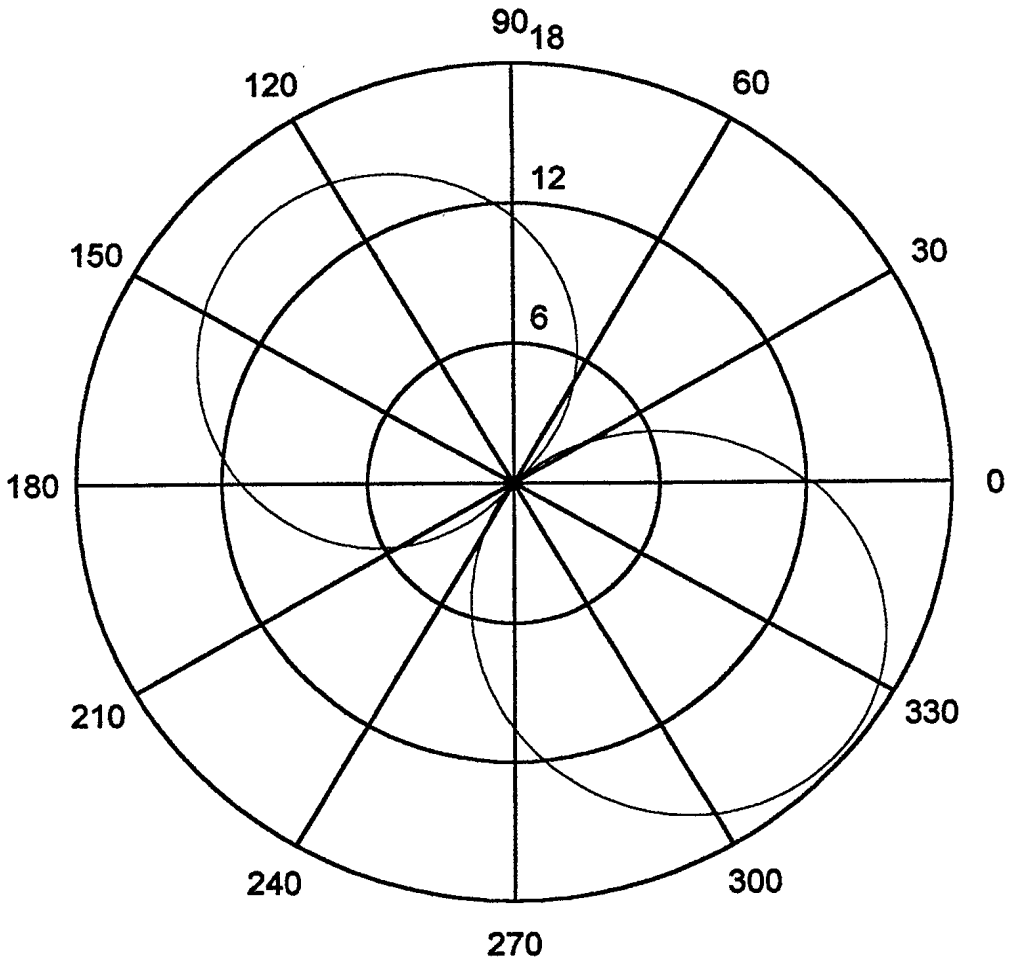

FIGURE 3.7: Field Pressures Produced by the CYLN1 Model Vibrating at the Fifth Coupled Natural Frequency

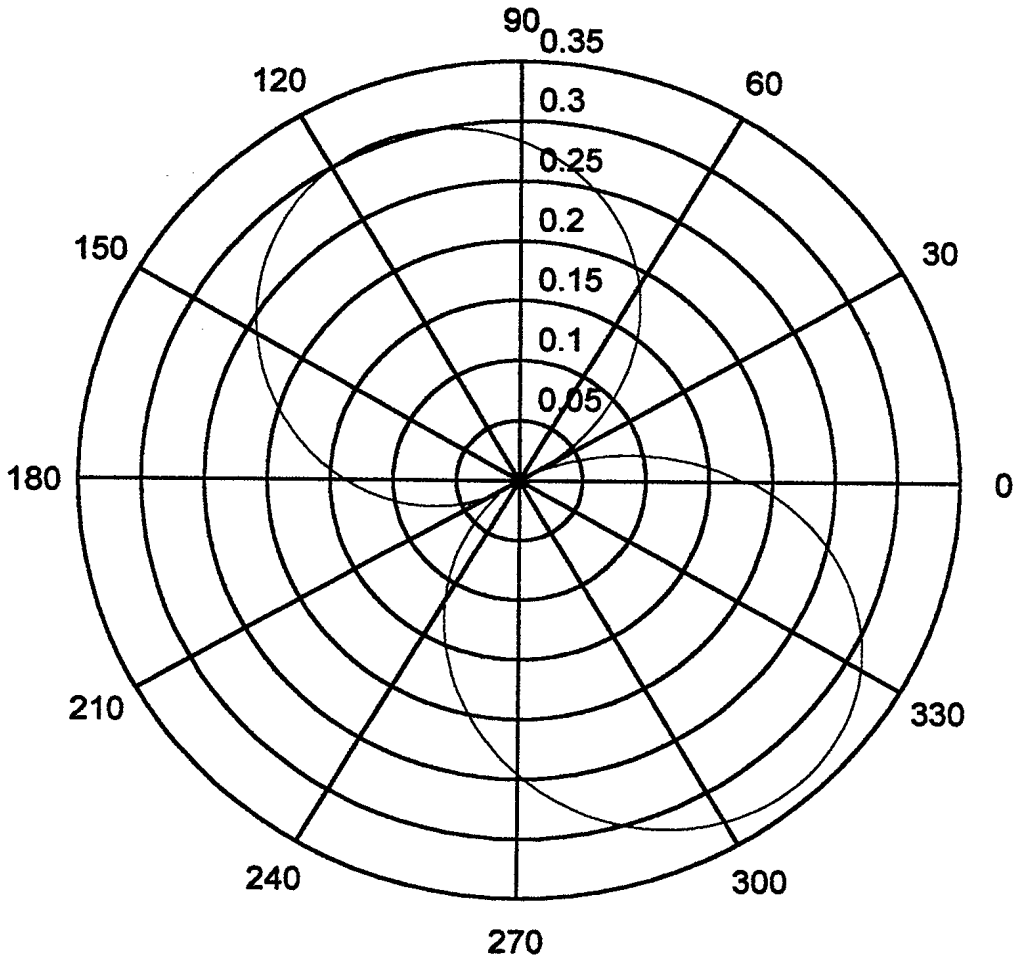

FIGURE 3.8: Field Pressures Produced by the CYLN1 Model Vibrating at the Sixth Coupled Natural Frequency

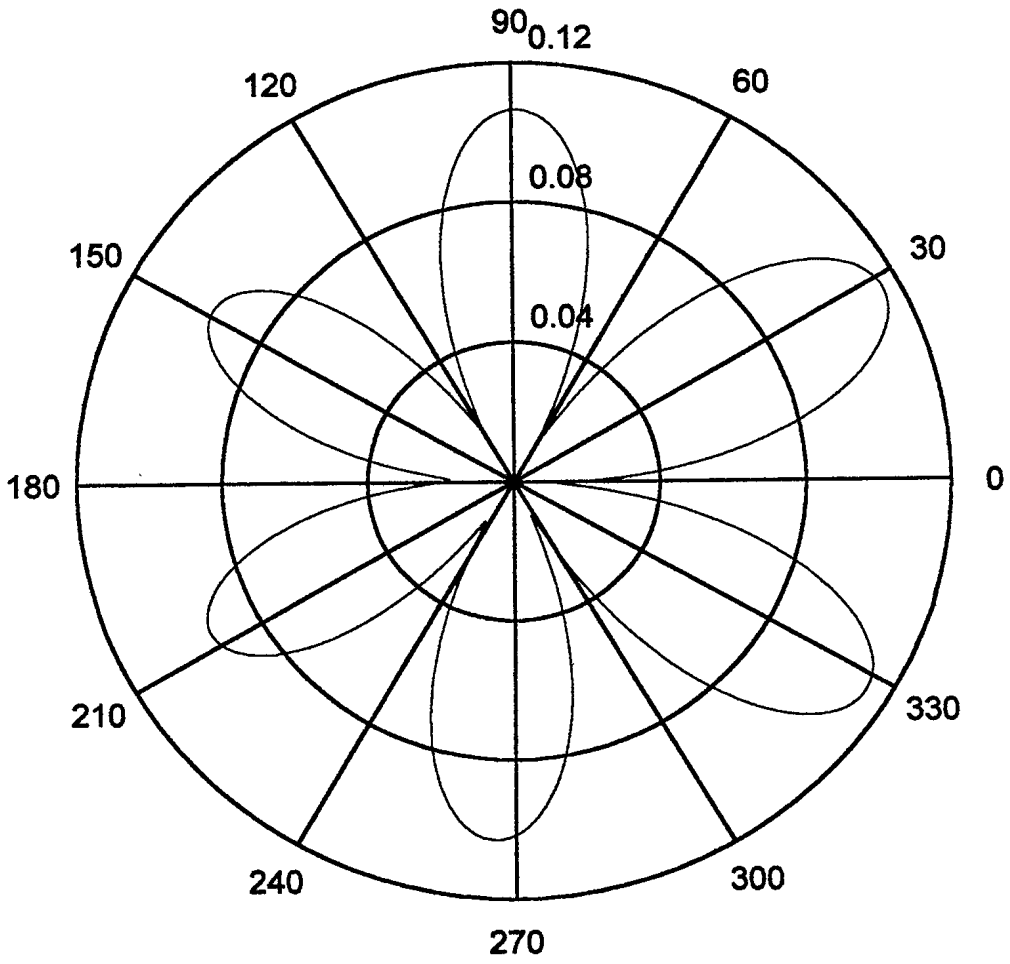

FIGURE 3.9: Field Pressures Produced by the CYLN2 Model Vibrating at the First Coupled Natural Frequency

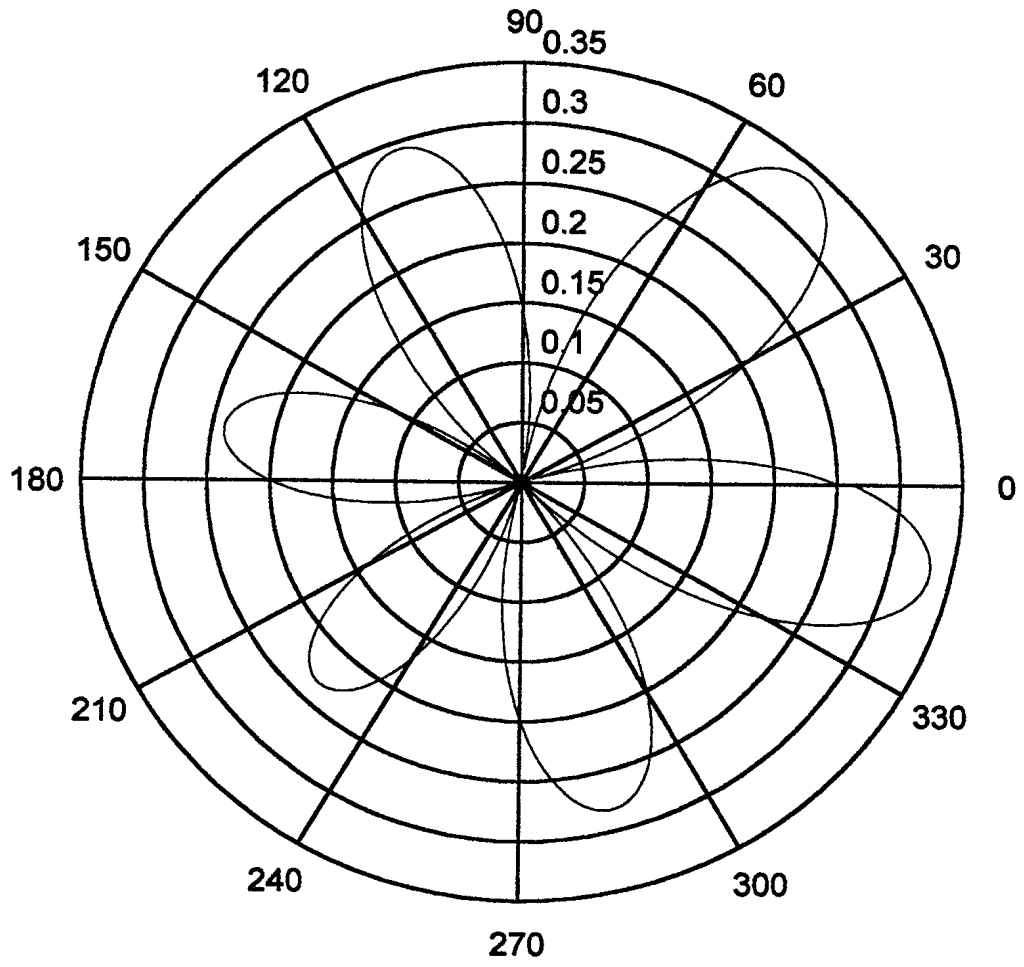

FIGURE 3.10: Field Pressures Produced by the CYLN2 Model Vibrating at the Second Coupled Natural Frequency

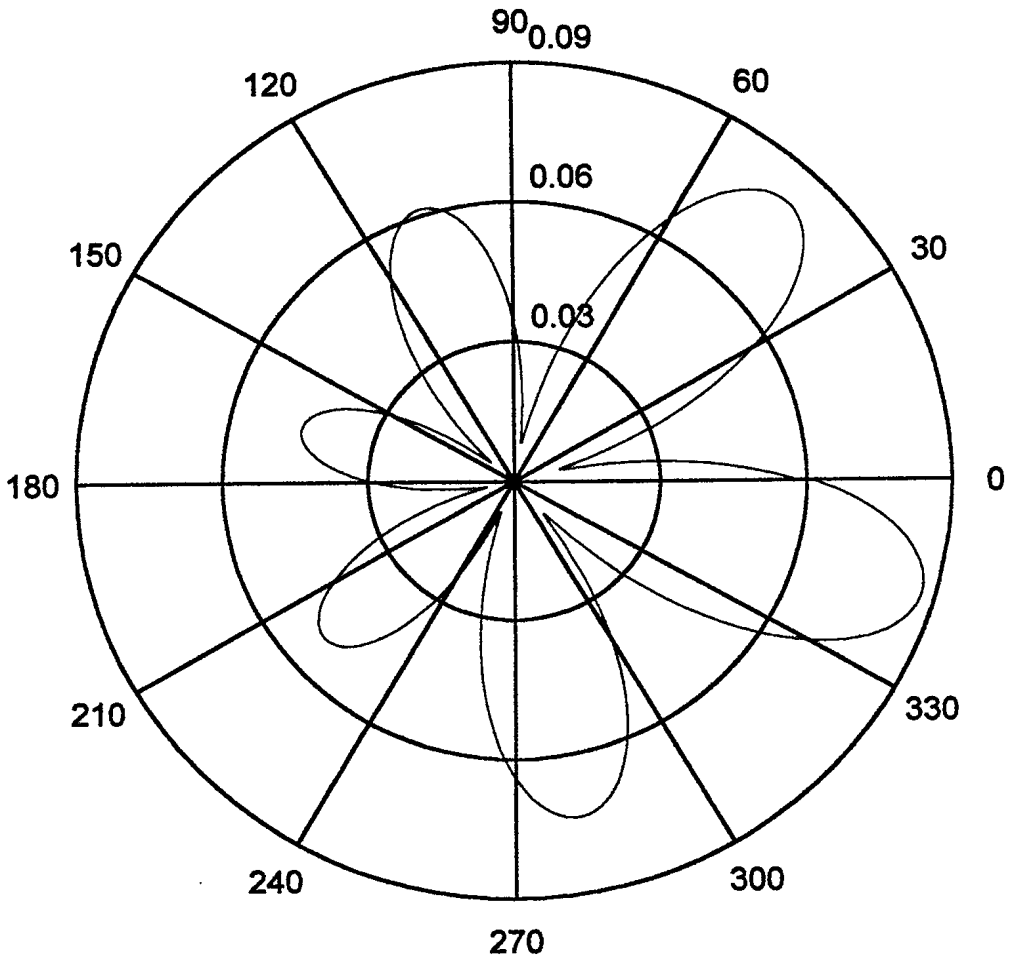

FIGURE 3.11: Field Pressures Produced by the CYLN2 Model Vibrating at the Third Coupled Natural Frequency

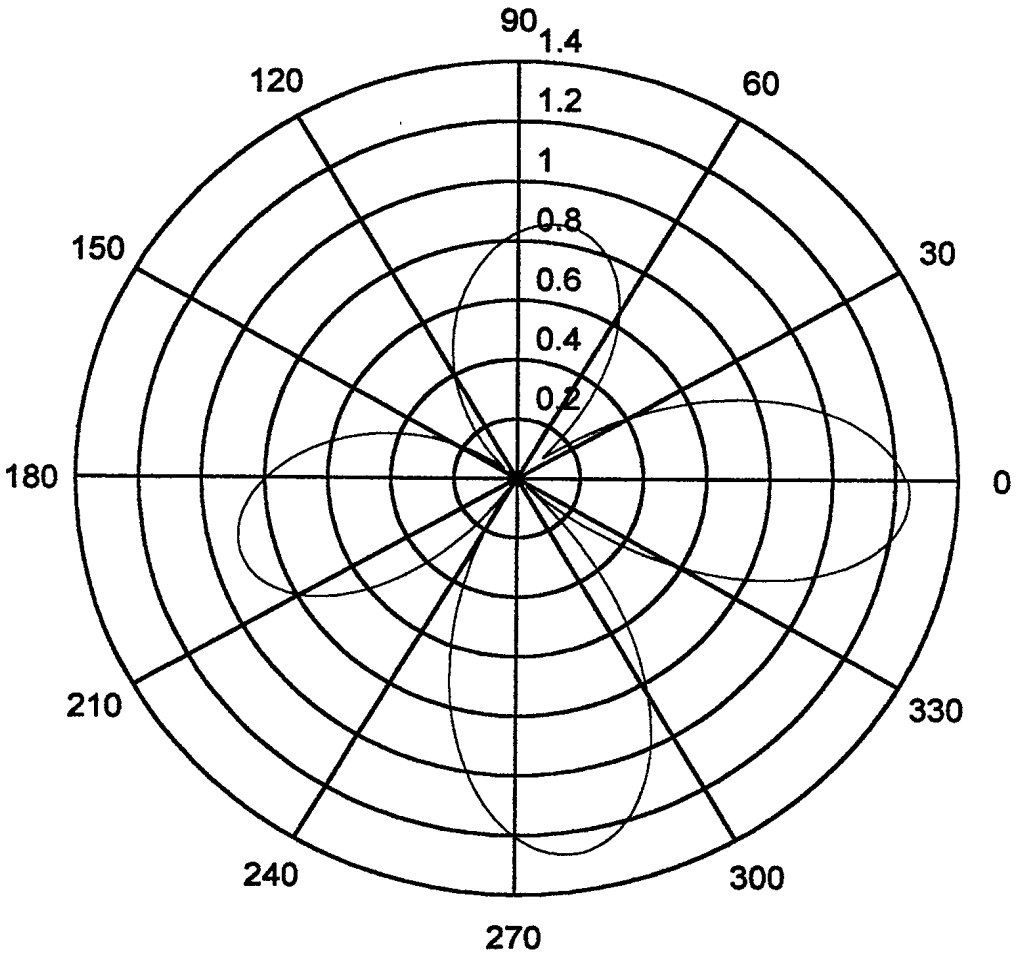

FIGURE 3.12: Field Pressures Produced by the CYLN2 Model Vibrating at the Fourth Coupled Natural Frequency

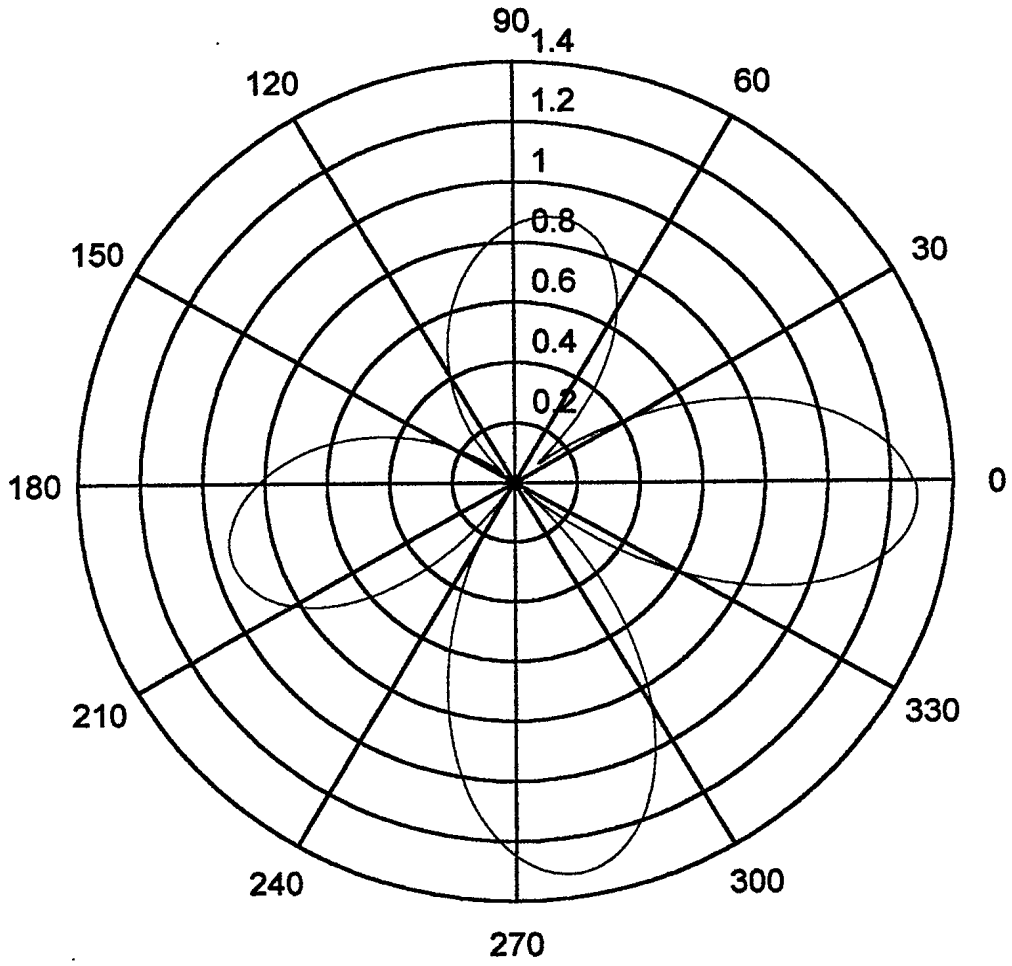

FIGURE 3.13: Field Pressures Produced by the CYLN2 Model Vibrating at the Fifth Coupled Natural Frequency

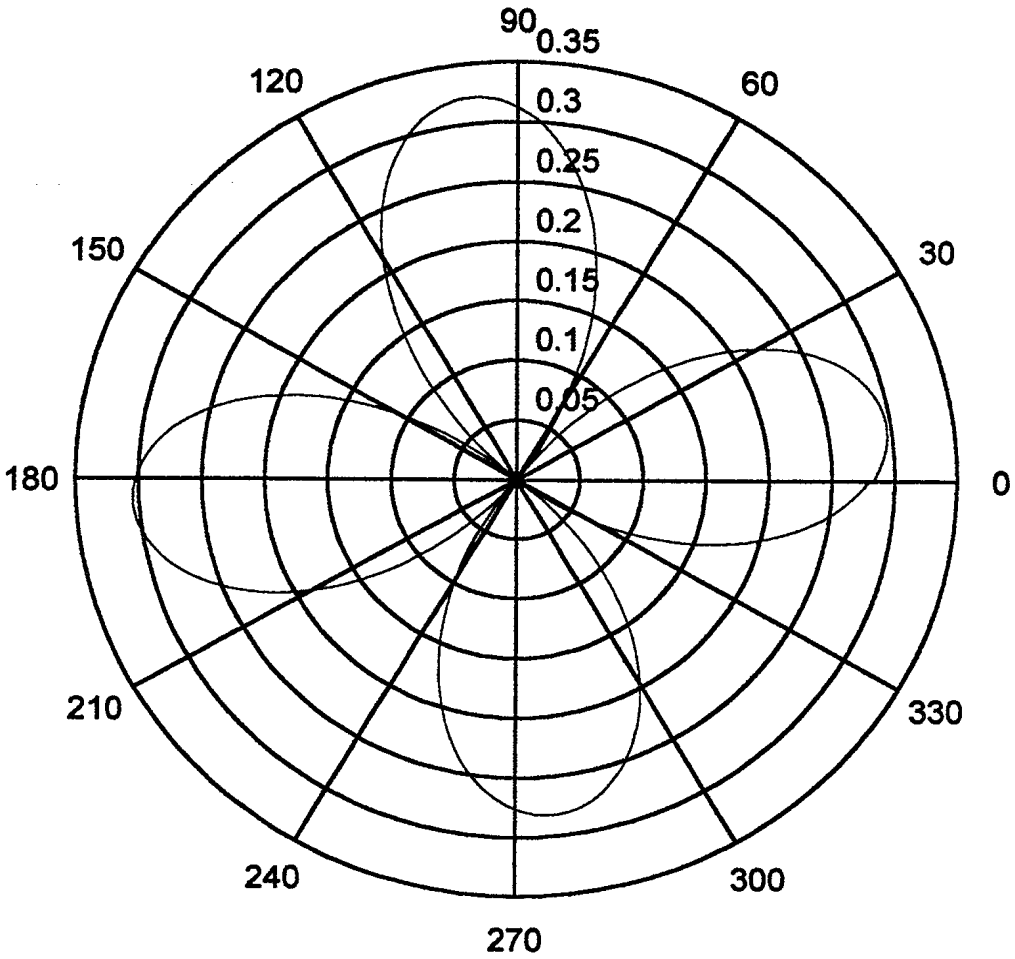

FIGURE 3.14: Field Pressures Produced by the CYLN2 Model Vibrating at the Sixth Coupled Natural Frequency

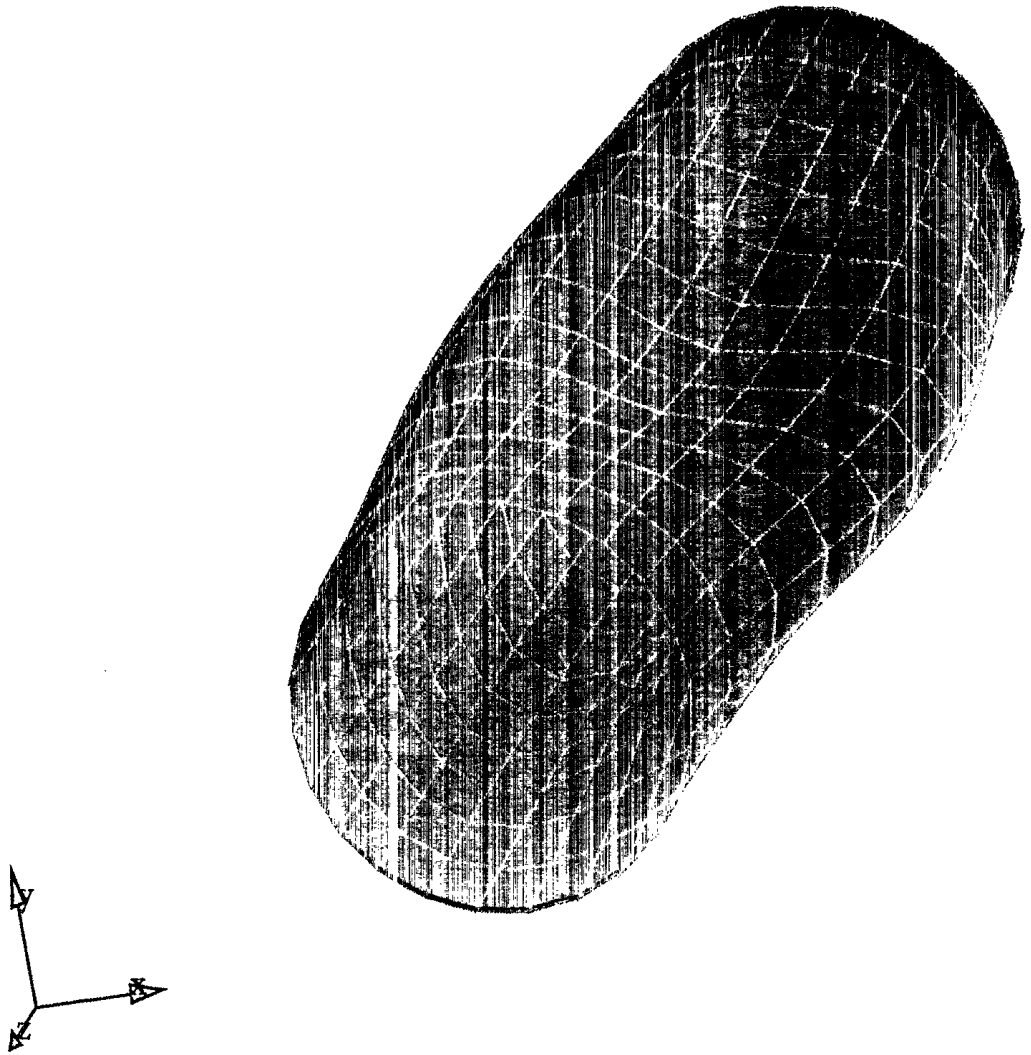

FIGURE 3.15: Deformed Shape of the CYLN1 Model When Loaded at the First Wet Natural Frequency

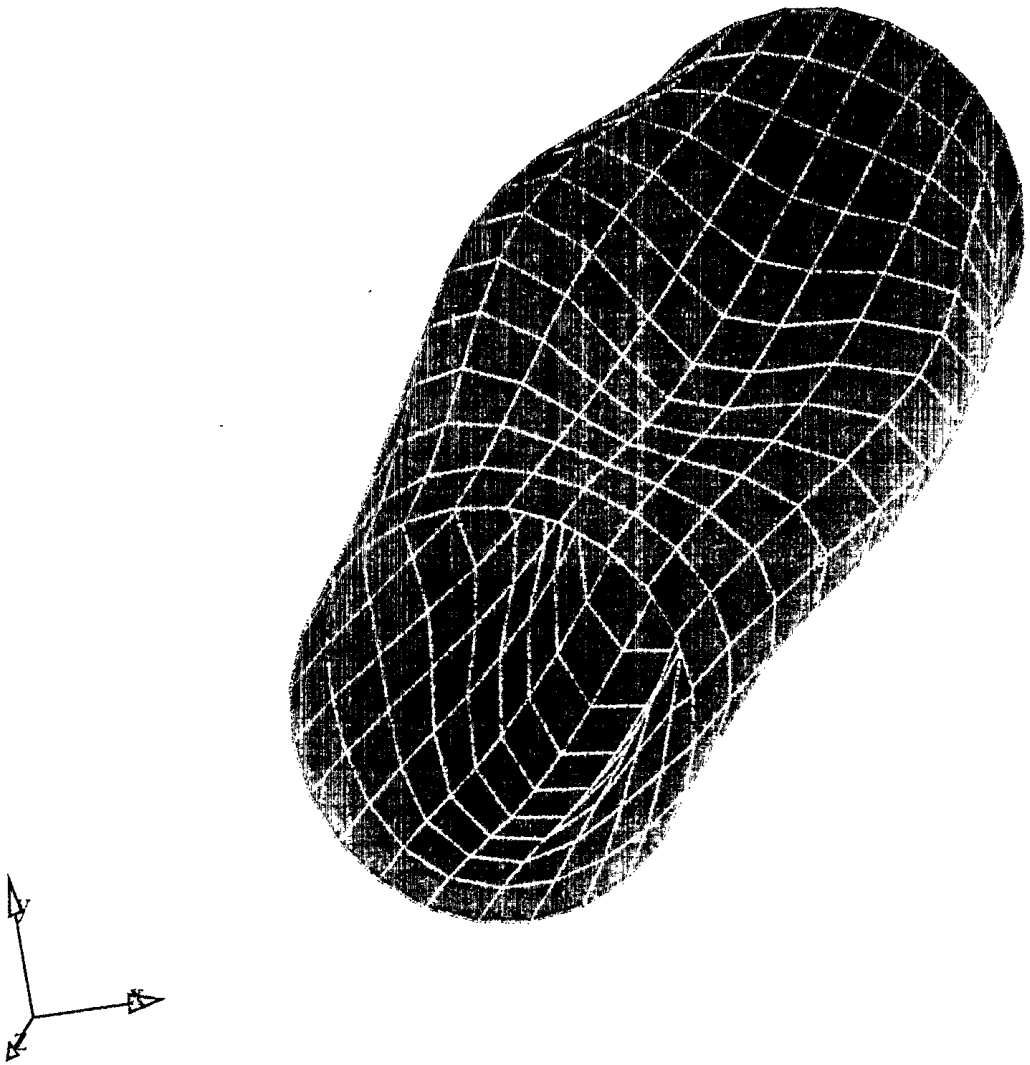

FIGURE 3.16: Deformed Shape of the CYLN1 Model When Loaded at the Second Wet Natural Frequency

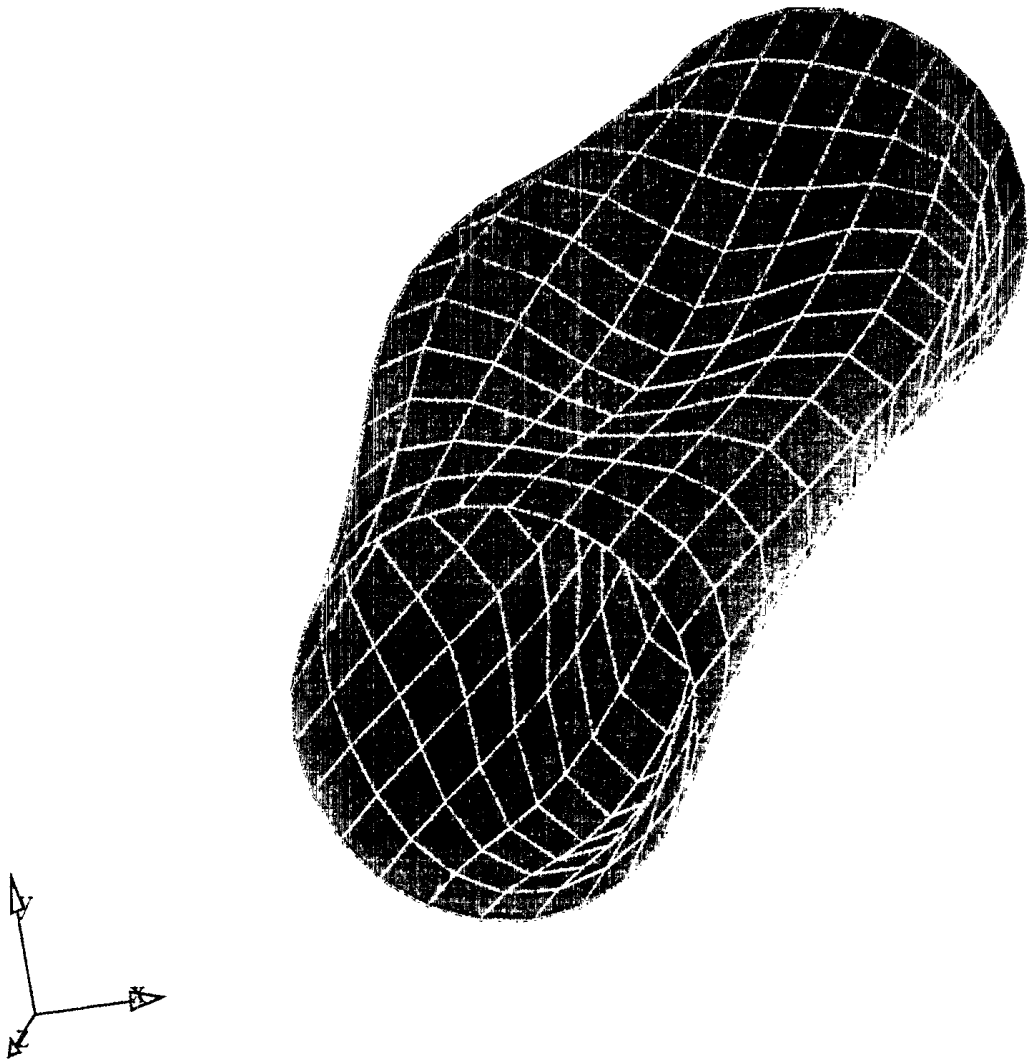

FIGURE 3.17: Deformed Shape of the CYLN1 Model When Loaded at the Third Wet Natural Frequency

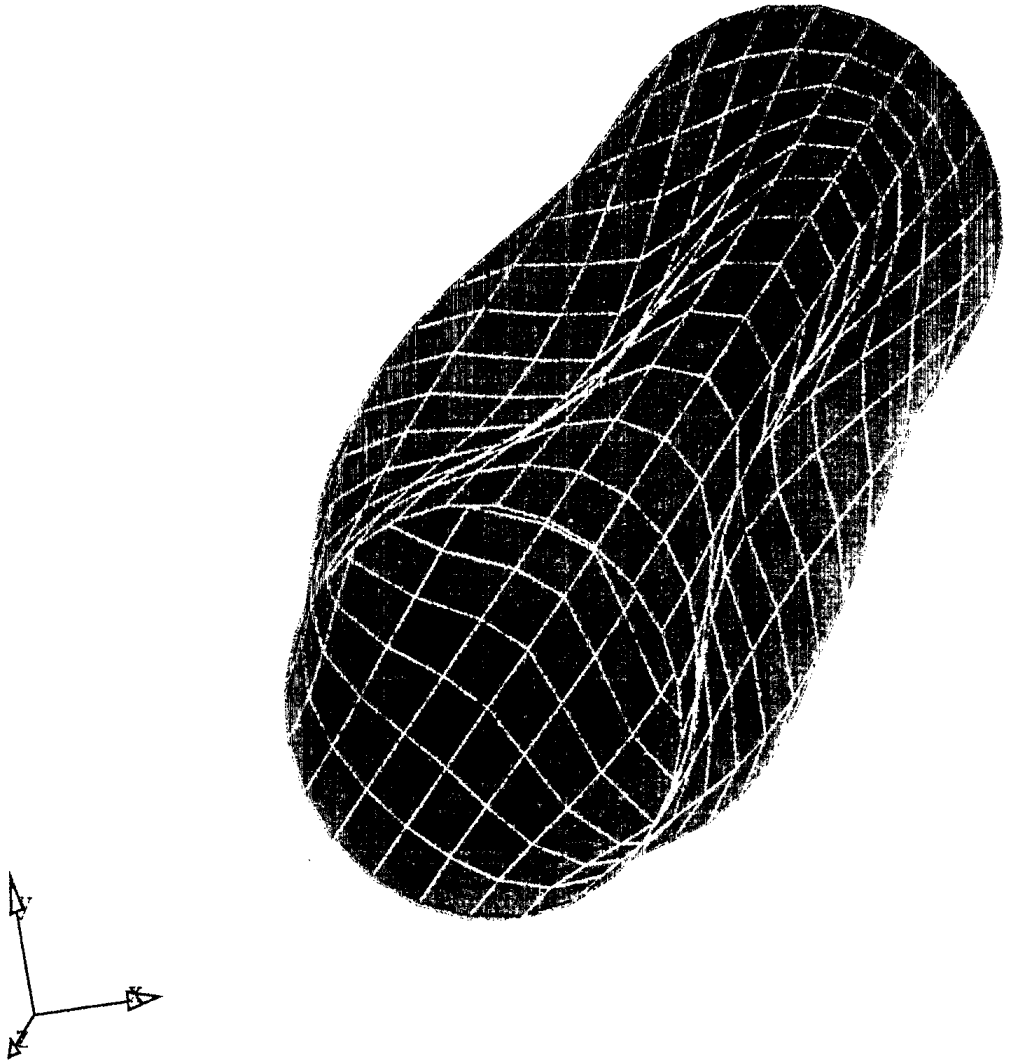

FIGURE 3.18: Deformed Shape of the CYLN1 Model When Loaded at the Fourth Wet Natural Frequency

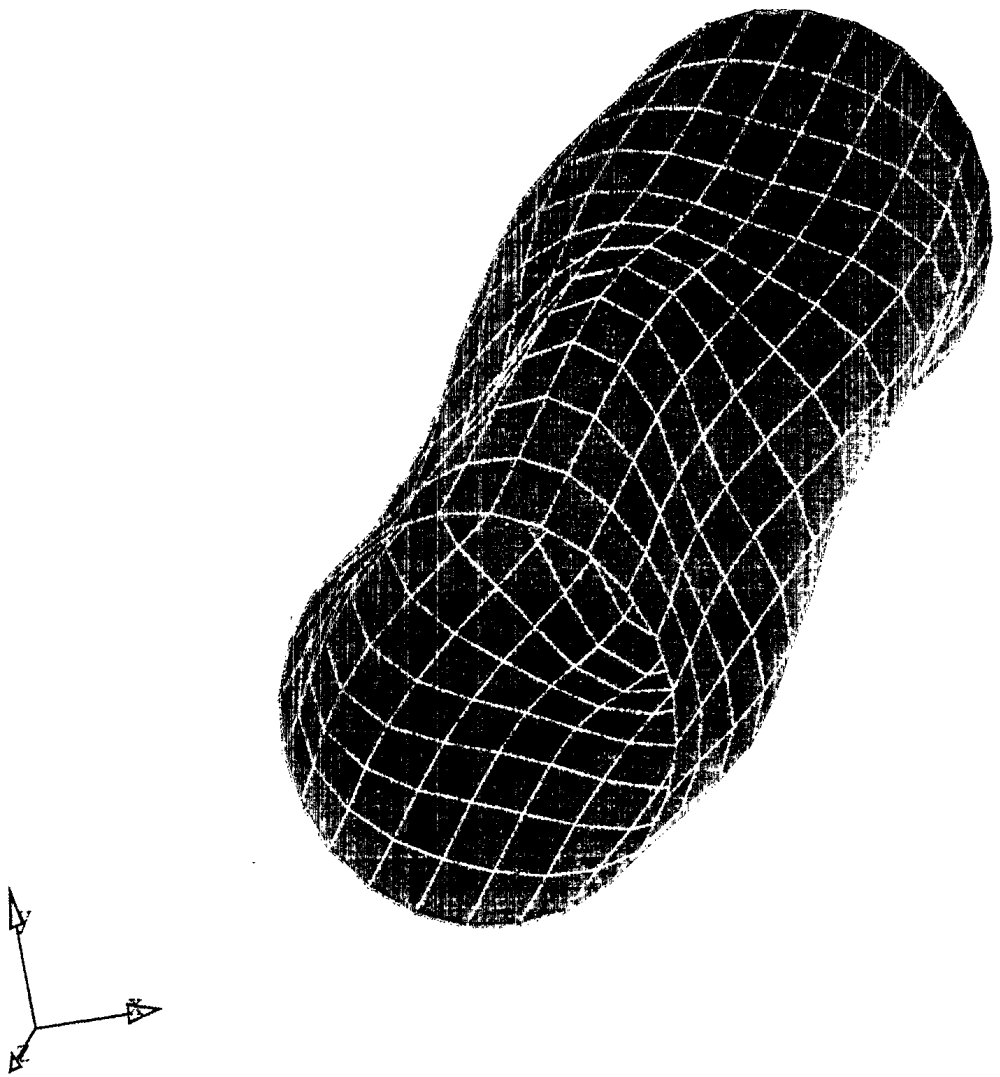

FIGURE 3.19: Deformed Shape of the CYLN1 Model When Loaded at the Fifth Wet Natural Frequency

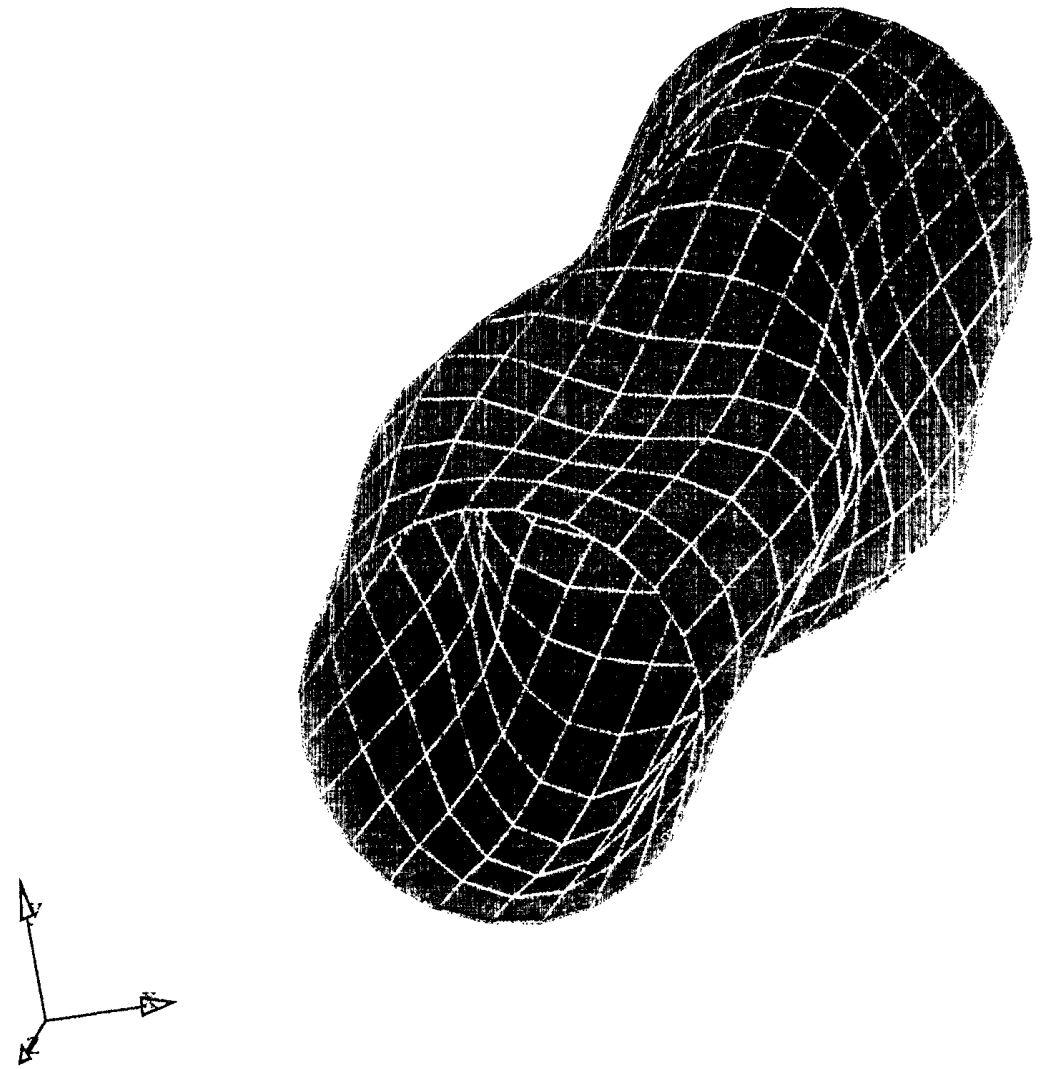

FIGURE 3.20: Deformed Shape of the CYLN1 Model When Loaded at the Sixth Wet Natural Frequency

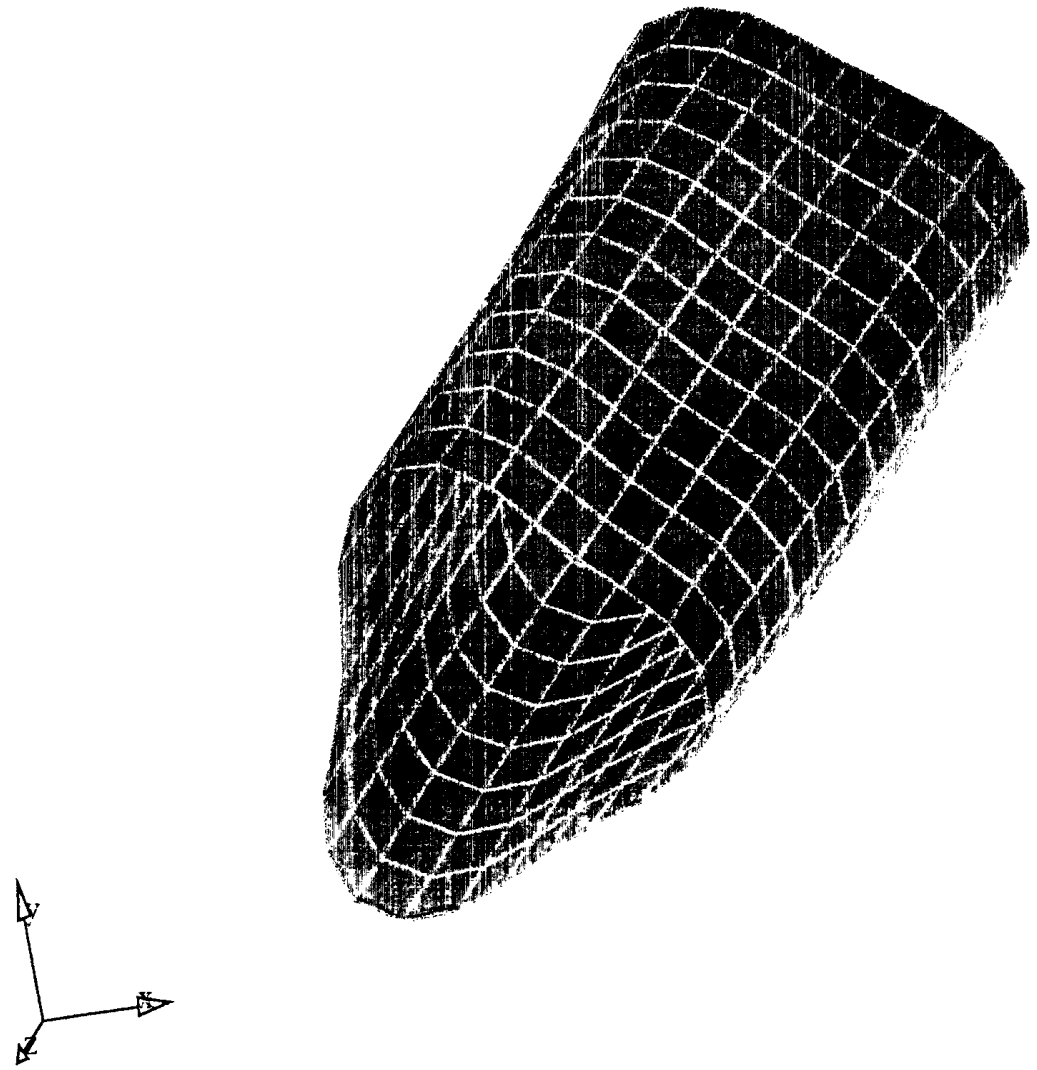

FIGURE 3.21: Deformed Shape of the CYLN2 Model When Loaded at the First Wet Natural Frequency

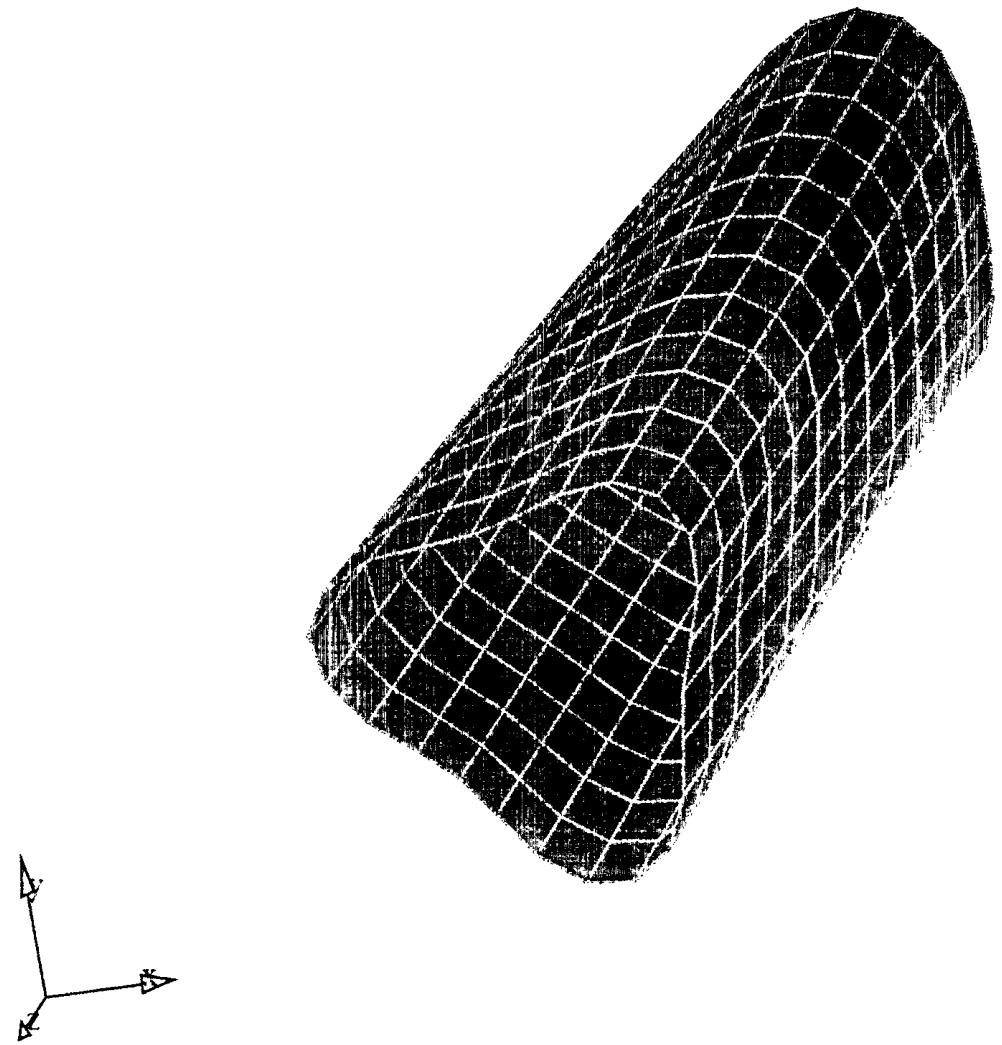

FIGURE 3.22: Deformed Shape of the CYLN2 Model When Loaded at the Second Wet Natural Frequency

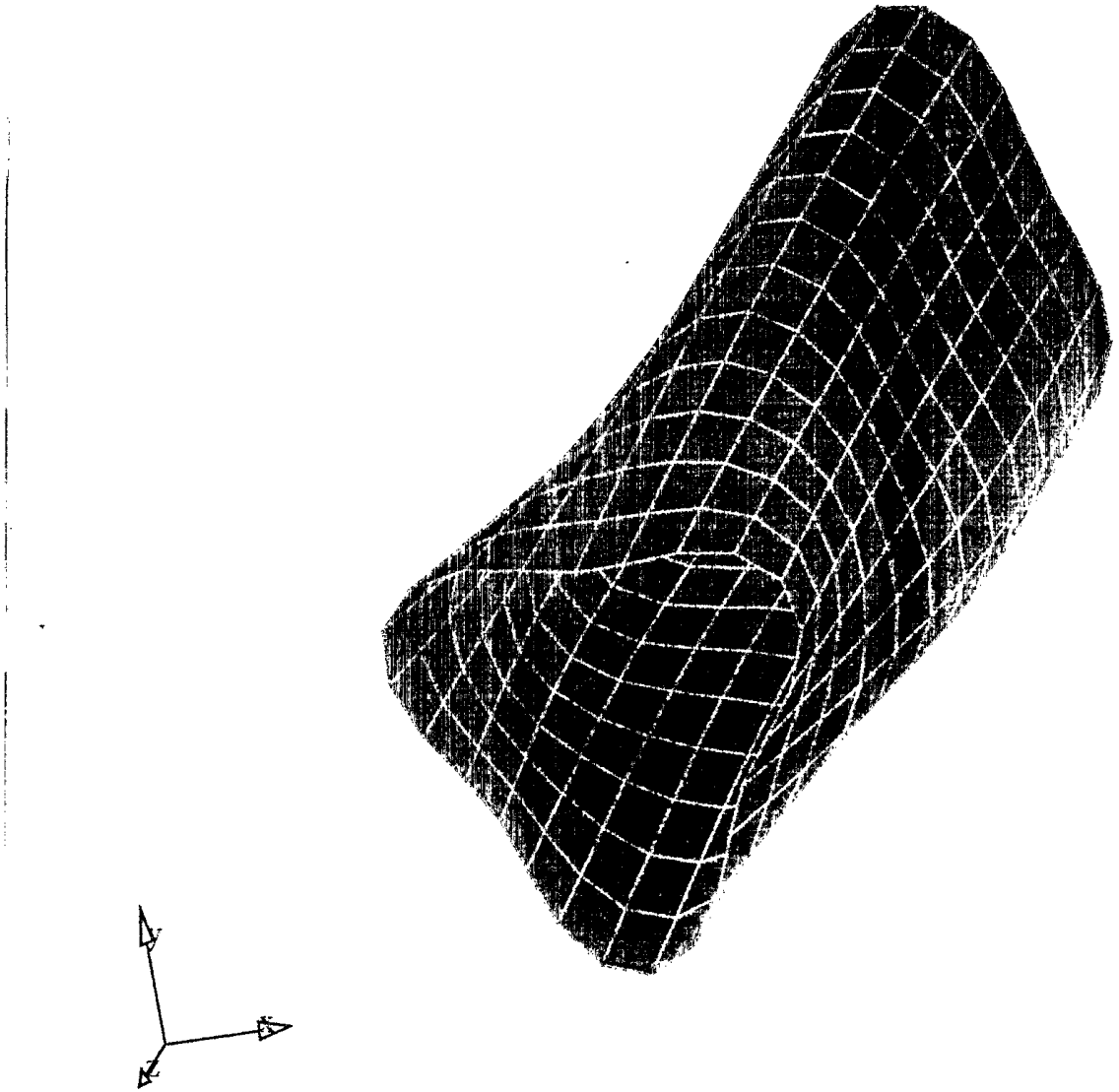

FIGURE 3.23: Deformed Shape of the CYLN2 Model When Loaded at the Third Wet Natural Frequency

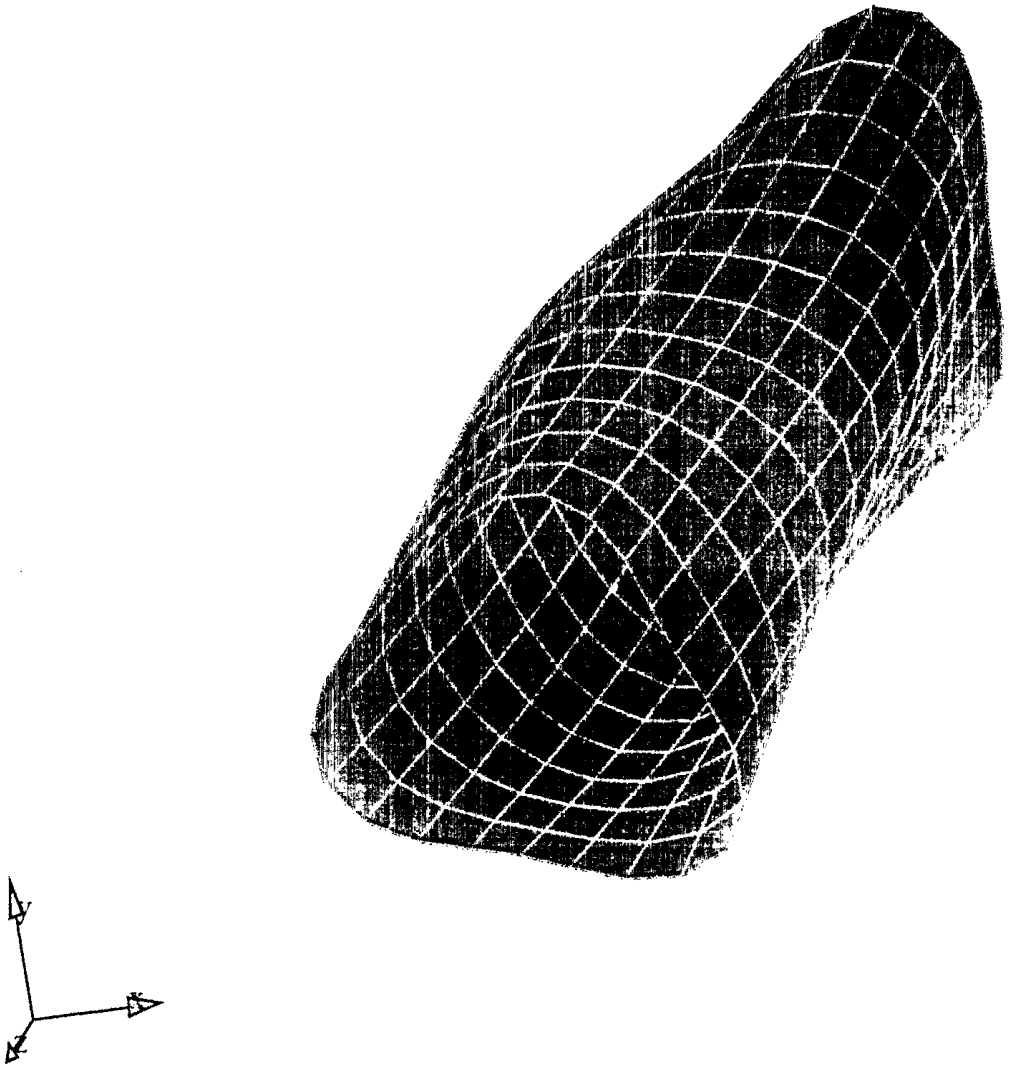

FIGURE 3.24: Deformed Shape of the CYLN2 Model When Loaded at the Fourth Wet Natural Frequency

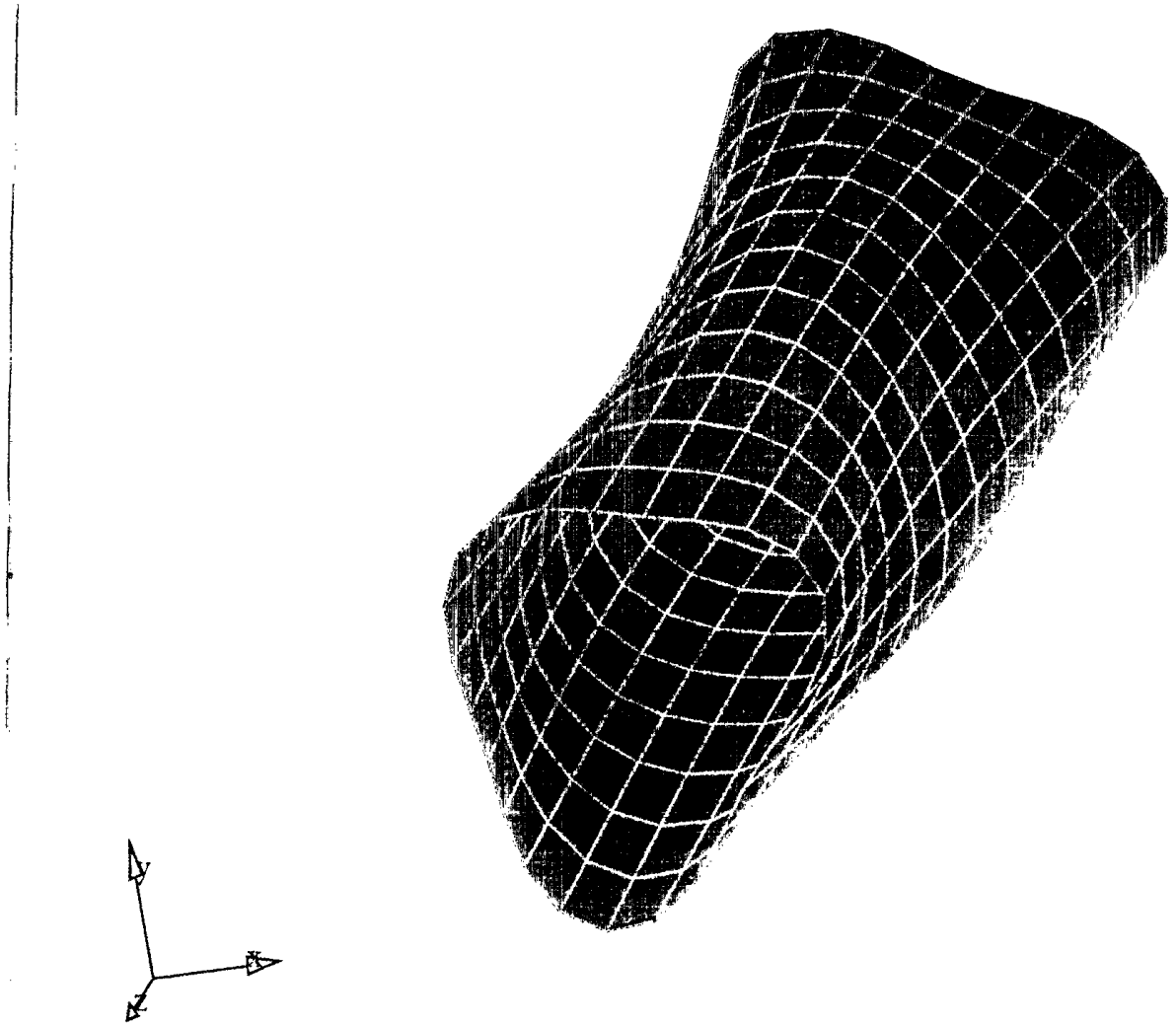

FIGURE 3.25: Deformed Shape of the CYLN2 Model When Loaded at the Fifth Wet Natural Frequency

4. INCORPORATION OF THE AVAST FLUID MODELLER INTO THE COUPLE CODE

4.1 Introduction

The COUPLE [1] program was developed primarily for the prediction of natural frequencies of coupled fluid/structure systems. The model of the structure is generated for a standard structural analysis and is run through the VAST program to the point where the mass and stiffness matrices are generated. The corresponding fluid model is generated and run through COUPLE to assemble the fluid stiffness and mass matrices. COUPLE then reads in the structural matrices and performs any necessary modifications, such as inverses or transposes to the two sets of matrices, before combining them in the desired form of assembled fluid/structure stiffness and mass matrices. The assembled stiffness and mass matrices are then run through the VAST program for decomposition and calculation of the coupled fluid/structure natural frequencies and mode shapes. Further analysis of the coupled system using the VAST frequency response capability and commercial boundary element code BEMAP allows for the prediction of acoustic radiation from models excited by external loads.

Unfortunately, the version of BEMAP presently available at DREA cannot support the relatively large structural models currently of interest to the research staff. As a result, it was proposed that a modified version of the AVAST fluid modeller be incorporated into the COUPLE program. Since AVAST has no effective limit on the number of fluid degrees-of-freedom, models such as the one currently under development of the DREA barge facility may now be considered using an upgraded version of COUPLE suite.

4.2 AVASTC Acoustic Modelling Routines

In order to provide an acoustic modelling capability for users of the COUPLE program, a modified version of the AVAST code, named AVASTC (AVAST-COUPLE), is now available. The AVASTC module ACSURF allows users to calculate acoustic pressures on the wet surface of the radiating structure by simply requiring the user to supply the names of the files which store the structural displacements generated via a VAST frequency aresponse analysis [4] and the geometric description of the wet structural surface (for details on the fluid geometry file, see Reference [20]). Once these surface acoustic pressures have been established, sound pressure levels throughout the fluid domain may be computed using the ACFIELD module. ACFIELD requires only the five character

prefix of the file (having the extension .EFP) which stores the cartesian coordinates of the locations where field pressures are to be calculated. ACFIELD will then produce an ASCII file, having the extension .FPR, which contains the real and imaginary components of the acoustic field pressures.

5. REFERENCES

[1] L.E. Gilroy and S. Tang, "An Improved Finite Element Based Method for Coupled Fluid/Structure Eigenvalue Analysis", DREA Technical Memorandum 91/209, 1991.

[2] D.P. Brennan, M.W. Chernuka and M.E. Norwood, "Acoustic Radiation From Submerged Elastic Structures," Martec Technical Report TR-92-11, June 1992.

[3] D.P. Brennan and M.W. Chernuka, "Acoustic Radiation From Submerged Elastic Structures — Phase II Developments," Martec Technical Report TR-92-16, July 1992.

[4] "Vibration and Strength Analysis Program (VAST): User's Manual, 6.1," Martec Limited, Halifax, NS, December 1993.

[5] S.M. Kirkup and D.J. Henwood, "Methods for Speeding up the Boundary Element Solutions of Acoustic Radiation Problems," Transactions of the ASME, Vol. 114, pp. 374-380, July 1992.

[6] S. Amini and S.M. Kirkup, "Solution of the Helmholtz Equation in the Exterior Domain by Elementary Boundary Integral Methods," J. Comp. Physics, Vol. 118, pp. 208-221, 1995.

[7] J.A. DeRuntz and T.L. Geers, "Added Mass Computation by the Boundary Integral Method," Int. J. Num. Meth. Eng., Vol. 12, pp. 531-549, 1978.

[8] A.F. Seybert, "An Advanced Computational Method for Predicting and Scattering of Acoustic Waves in Three-Dimensions," JASA, Vol. 77, No. 2, pp. 362-368.

[9] L.E. Gilroy and D.P. Brennan, "Predicting Radiated Noise From Submerged and Floating Structures," Presented at the Third Canadian marine Hydrodynamics and Structures Conference, Halifax, NS, 1995.

[10] S.M. Kirkup and S. Amini, "Modal Analysis of Acoustically-Loaded Structures Via Integral Equation Methods," Comp. Struct. Vol. 40, No. 5, pp. 1279-1285, 1991.

[11] S.M. Kirkup and S. Amini, "Solution of the Helmholtz Eigenvalue Problem Via the Boundary Element Methods," Int. J. Num. Meth. Eng., Vol. 36, pp. 321-330, 1993.

[12] P.K. Banerjee, S. Ahmad and H.C. Wang, "A New BEM Formulation for the Acoustic Eigenfrequency Analysis," Int. J. Num. Meth. Eng., Vol. 26, pp. 1299-1309, 1988.

[13] B.S. Garbow, "EISPACK — for the Generalized Eigenvalue Problem," Applied Mechanics Division, Algonne National Laboratory, 1980.

[14] J.P. Coyette and K.R. Fyfe, "An Improved Formulation for Acoustic Eigenmode Extraction From Boundary Element Models," Presented at the Winter Annual Meeting of the American Society of Mechanical Engineers, San Francisco, CA, 1989.

[15] C. Rajakumar and A. Ali, "Acoustic Boundary Element Eigenproblem with Sound Absorption and its Solution Using Lańczos Algorithm," Int. J. Num. Meth. Eng., Vol. 36, pp. 3957-3972, 1993.

[16] "LAPACK User's Guide, Release 2.0," Society for Industrial and Applied Mathematics (SIAM), Philadelphia, PA, 1994.

[17] C.B. Moler and G.W. Stewart, "An Algorithm for Generalized Matrix Eigenvalue Problems," SIAM J. Numer. Anal., Vol. 10, pp. 241-256, 1973.

[18] S. Kirkup, personal communication, 1996.

[19] L.E. Gilroy, "Natural Frequency and Radiated Noise Measurements on a Ring-Stiffened Cylinder-Experimental Data Annex," DREA Technical Memorandum, december, 1993.

[20] D.P. Brennan, "AVAST User's Manual," Martec Limited, Halifax, NS, 1996.

UNCLASSIFIED

SECURITY CLASSIFICATION OF FORM
(highest classification of Title, Abstract, Keywords)

DOCUMENT CONTROL DATA

(Security classification of title, body of abstract and indexing annotation must be entered when the overall document is classified)

1. ORIGINATOR (The name and address of the organization preparing the document. Organizations for whom the document was prepared, e.g. Establishment sponsoring a contractor's report, or tasking agency, are entered in section 8.)

MARTEC Ltd.
1888 Brunswick St., Suite 400
Halifax, Nova Scotia, B3J 3J8

2. SECURITY CLASSIFICATION (Overall security of the document including special warning terms if applicable.)

UNCLASSIFIED

3. TITLE (The complete document title as indicated on the title page. Its classification should be indicated by the appropriate abbreviation (S,C,R or U) in parentheses after the title.)

Enhancements to AVAST

4. AUTHORS (Last name, first name, middle initial. If military, show rank, e.g. Doe, Maj. John E.)

Brennan, D.P. and Chernuka, M.W.

5. DATE OF PUBLICATION (Month and year of publication of document.)

March 1996

6a. NO. OF PAGES (Total containing information. Include Annexes, Appendices, etc.)

56

6b. NO. OF REFS. (Total cited in document.)

20

6. DESCRIPTIVE NOTES (The category of the document, e.g. technical report, technical note or memorandum. If appropriate, enter the type of report, e.g. interim, progress, summary, annual or final. Give the inclusive dates when a specific reporting period is covered.)

Contractor Report

8. SPONSORING ACTIVITY (The name of the department project office or laboratory sponsoring the reseach and development. include the address.)

Defence Research Establishment Atlantic
P.O. Box 1012, Dartmouth, N.S. , Canada, B2Y 3Z7

9a. PROJECT OR GRANT NUMBER (If appropriate, the applicable research and development project or grant number under which the document was written. Please specify whether project or grant.)

Project 1.g.a

9b. CONTRACT NUMBER (If appropriate, the applicable number under which the document was written.)

W7707-5-3369/01-HAL

10a. ORIGINATOR'S DOCUMENT NUMBER (The official document number by which the document is identified by the originating activity. This number mrst be unique to this document.)

MARTEC Report No. TR-96-05

10b. OTHER DOCUMENT NUMBERS (Any other numbers which may be assigned this document either by the originator or by the sponsor.)

DREA Contractor Report 96/421

11. DOCUMENT AVAILABILITY (Any limitations on further dissemination of the document, other than those imposed by security classification)

(X) Unlimited distribution
( ) Distribution limited to defence departments and defence contractors; further distribution only as approved
( ) Distribution limited to defence departments and Canadian defence contractors; further distribution only as approved
( ) Distribution limited to government departments and agencies; futher distribution only as approved
( ) Distribution limited to defence departments; further distribution only as approved
( ) Other (please specify):

12. DOCUMENT ANNOUNCEMENT (Any limitation to the bibliographic annoucement of this document. This will normally correspond to the Document Availability (11). However, where futher distribution (beyond the audience specified in 11) is possible, a wider announcement audience may be selected.)

Full, unlimited

13. ABSTRACT (a brief and factual summary of the document. It may also appear elsewhere in the body of the document itself. It is highly desirable that the abstract of classified documents be unclassified. Each paragraph of the abstract shall begin with an indication of the security classification of the information in the paragraph (unless the document itself is unclassified) represented as (S), (C), (R), or (U). It is not necessary to include here abstracts in both official languages unless the text is bilingual).

The development and incorporation of the latest enhancements to the AVAST code are described. The purpose of this work was to make the modelling of the physical environment more realistic, while ensuring that the code runs as efficiently as possible. To this end, several new features have been added. These include the implementation of a four-noded acoustic panel element and the development of an eigenvalue extraction technique suitable for equations generated by the boundary integral equation method. In addition, the option to use structural response data generated by the COUPLE program has been incorporated.

14. KEYWORDS, DESCRIPTORS or IDENTIFIERS (technically meaningful terms or short phrases that characterize a document and could be helpful in cataloguing the document. They should be selected so that no security classification is required. Identifiers, such as equipment model designation, trade name, military project code name, geographic location may also be included. If possible keywords should be selected from a published thesaurus. e.g. Thesaurus of Engineering and Scientific Terms (TEST) and that thesaurus-identified. If it not possible to select indexing terms which are Unclassified, the classification of each should be indicated as with the title).

acoustic radiation
finite element
boundary element
prediction
computer
eigenvalue

#508057